9 The Infrared Galaxy

Ed Churchwell[1] · *Robert A. Benjamin*[2]
[1]Department of Astronomy, University of Wisconsin, Madison, WI, USA
[2]Department of Physics, University of Wisconsin - Whitewater, Whitewater, WI, USA

Abstract: As infrared surveys have reached optical-quality angular resolution, they have revealed new information on the stellar, interstellar, and star-formation components of the Galaxy. The distance to the Galactic center appears to be known to within 5%: $R_o = 8.0 \pm 0.4$ kpc. Measurements of the stellar scalelength of the disk, $R_d = 2$–4 kpc, continue to show a large range; the origin of this scatter needs to be understood. The exponential disk does not continue into the center of the Galaxy, with an inner radius of $R_h \sim 3$ kpc. Claims exist for a truncation, or change in scalelength, in the outer disk, but are not yet confirmed. The stellar disk is warped, with a similar nonsymmetric azimuthal dependence as the HI disk, but a lower amplitude and uncertain radial extent. There is extensive evidence for two non-axisymmetric structures in the inner galaxy: the Galactic bar (or triaxial bulge) and the Long Bar, which differ in angle by $\sim 20°$. The existence of an inner (nuclear) bar seems likely, but studies have not converged on its parameters. There is no compelling evidence for a ring in stellar mass, but a case can be made for a star-forming ring.

These surveys have also revealed the projected Galactic distribution of interstellar dust and shed light on the extinction and radiation properties of dust in different Galactic environments. We review the spatial distribution and wavelength dependence of extinction, the distribution and magnitude of PAH emission and stochastic and thermal dust emission, and different stages of massive star formation, e.g., infrared dust clouds (IRDCs), IR bubbles around HII regions, extended green objects (EGOs), and massive star formation regions, including evidence for triggered star formation. We briefly discuss what infrared observations tell us about evolved stars, including variable stars, asymptotic giant stars (AGB), planetary nebulae (PNe), Luminous Blue Variables (LBVs) and Wolf-Rayet stars, and supernova remnants. We end with a comparison of the limitations of optical, infrared, and radio surveys of the Galaxy that should be borne in mind.

Keywords: Galaxy:stellar content, Galaxy:structure, Infrared:general, Infrared:ISM, Infrared: stars, ISM: general, Stars:general, Survey

1 The Infrared Era of Galactic Astronomy

Among the most strikingly beautiful features of an optical panorama of the Milky Way (❯ *Fig. 9-1*) are the prominent dust lanes running along the Galactic plane. But in terms of making progress in understanding the structure of the Milky Way, particularly the stellar structure, dust has been the enemy. Because of the dust and the vast spread in distance of objects in a given direction, less is known about the large-scale structure and kinematics of our Galaxy, the Milky Way, than many nearby spiral galaxies. Determination of the extent and morphology of the Galaxy presents much the same problem faced by a hiker lost in a foggy forest. To determine the extent and shape of the forest, somehow the hiker has to find a way to see all the way to the edge of the forest and estimate distances along the line of sight.

Until the mid-1980s, our knowledge of the extent and structure of the Milky Way was almost exclusively from large-scale radio surveys of HI and CO gas tracers. However, certain fundamental limitations frustrated one of the ultimate goals of these surveys: the creation of a reliable map of the distribution of interstellar gas in the Milky Way. The recent discovery of the *Far Three-Kiloparsec Arm* (Dame and Thaddeus 2008) provides a striking example of these limitations. This structure is comparable in kinematics, atomic and molecular mass to the *Near Three-Kiloparsec Arm* (van Woerden et al. 1957). Its existence was predicted by
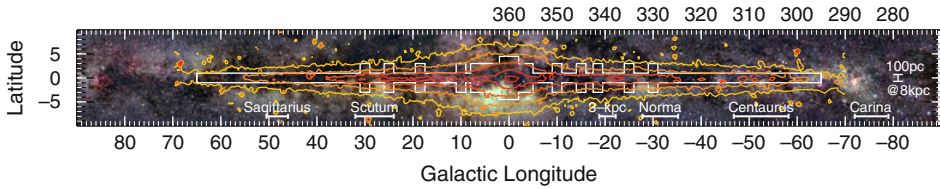
◼ Fig. 9-1

Optical panorama of the inner Milky Way (Mellinger **2009**). The patchy optical emission can be compared with the relatively smooth mid-infrared light observations of COBE/DIRBE 4.9 μm, shown in contours of logarithmic intensity (MJy/sr). The area covered by the original GLIMPSE survey, with $|b| < 1°$ except for certain longitude ranges, is shown in white. At a distance of 8 kpc, 1° corresponds to 140 pc. The "historical" longitude ranges for spiral arm tangencies are taken from Englmaier and Gerhard (**1999**). The main bar (or triaxial bulge) of the Galaxy extends from $l \sim 12°$ to about $-8°$. The Long Bar extends from $l = 30°$ to about $-15°$

Oort (1977) and more recent models of gas flow in a barred potential, c.f. Merrifield (2004). Yet it eluded detection for more than half a century! Why? Ultimately, the limitations in the angular resolution of even the most recent surveys, as well as the difficulties of converting longitude-velocity diagrams into longitude-distance diagrams, obscured this structure for many years.

It should also be noted that these pioneering surveys of HI and CO map only one component of the Galaxy: the interstellar gas. Observations of extragalactic systems show that the distribution of interstellar gas, of star formation, and of the stellar mass of a single spiral galaxy can be strikingly different (Block and Wainscoat 1991); their interrelationship contains information on how galaxies work as star formation factories.

In the last three decades, infrared surveys of the Galaxy have begun to shed new light on the global distribution, and differences in the distributions, of these three components of the Galaxy. In this review, we divide the infrared regime into the near-infrared (NIR) bands (1–2.5 μm), the mid-infrared (MIR) bands (2.5–50 μm), and the far-infrared (FIR) bands (50–500 μm). The near-infrared bands contain information about the distribution of stars throughout the galaxy as well as the physical nature and spatial distribution of dust extinction. The far-infrared bands provide constraints on the distribution and physical state of dust emission throughout the Galaxy. The mid-infrared bands have the optimum combination of low extinction and low diffuse emission needed to study the stellar content of the Galaxy, but are also ideal for studying the emission of polycyclic aromatic hydrocarbons (PAHs) and thermal emission from very small dust grains.

1.1 A Survey of Surveys

Since the 1980s, our knowledge of the Galaxy's structure and content has vastly expanded as a result of the opening of the infrared frontier. Much of this progress has come as a result of numerous surveys. ❯ *Table 9-1* contains basic information on these surveys. ❯ *Figure 9-2* compares their point source sensitivities. The conversion from flux units (Janskys=Jy) to magnitudes for different near- and mid-infrared surveys is given in ❯ *Table 9-2*.

⬛ Table 9-1

Summary of infrared surveys[a]

Survey	Wavebands (μm)	Resolution (″)	Coverage	Sensitivity (mJy)	Website
DENIS	0.97, 1.22, 2.16	1-3	$\delta = +2$ to $-88°$	0.2, 0.8, 2.8	cdsweb.u-strasbg.fr/denis.html
2MASS	1.22, 1.65, 2.16	2	all-sky	0.4, 0.5, 0.6	www.ipac.caltech.edu/2mass
UKIDSS-GPS[b]	1.22, 1.65, 2.16	0.5	$l = -2$ to $107°$, 142 to $230°$[c]	0.016, 0.023, 0.017	www.ukidss.org
GLIMPSE	3.6, 4.5, 5.8, 8.0	≤ 2	$|l| \leq 65°$, $|b| \lesssim 1°$[d]	0.2, 0.2, 0.4, 0.4	www.astro.wisc.edu/glimpse
GLIMPSE360	3.6, 4.5	≤ 2	$l = 65° - 255°$, $|b| \lesssim 2°$	0.012, 0.018	www.astro.wisc.edu/glimpse
WISE	3.4, 4.6, 12, 22	6, 6, 6, 12	all-sky	0.08, 0.1, 1, 6	wise.ssl.berkeley.edu
MSX	4.1, 8.3, 12, 14, 21	18.3	$l = 0-360°$, $|b| \leq 5°$	10000, 100, 1100, 900, 200	www.ipac.caltech.edu/ipac/msx
MIPSGAL	24, 70	6, 18	$|l| = 0-65°$, $|b| \lesssim 1°$	2, 75	mipsgal.ipac.caltech.edu
ISOGAL	7, 15	6	$|l| \leq 60°$, $|b| \leq 1°$[e]	15, 10	www.isogal.iap.fr/
IRAS	12, 24, 60, 100	25–100	all-sky	350, 650, 850, 3000	irsa.ipac.caltech.edu/IRASdocs
Akari	8.5, 20, 62.5, 80, 155, 175	5–44	all-sky	20-100	www.ir.isas.ac.jp
Herschel/Hi-GAL	70, 170, 250, 350, 500	5, 13, 18, 25, 36	$|l| = 0-60°$, $|b| \leq 1°$	18, 27, 13, 18, 15	hi-gal.ifsi-roma.inaf.it/higal
COBE/DIRBE[f]	1.25–240	0.7°	all-sky	0.01-1.0 MJy sr^{-1}	space.gsfc.nasa.gov/astro/cobe

[a] See text for appropriate references for these surveys

[b] Much of the remainder of the Galactic Plane will be covered with similar depth and resolution in the five-band near-infrared survey VVV (Minniti et al. 2010)

[c] $l = -2$ to $15°$ has thickness $|b| < 2°$, otherwise the thickness is $|b| < 5°$. The longitude range $l = 142° - 230°$ is also covered

[d] GLIMPSE also has vertical extensions up to $|b| = 4°.5$ for selected longitudes. GLIMPSE style coverage was used for the *Spitzer* Vela-Carnina survey from $l = 295° - 255°$

[e] Survey contained only selected fields in this region, totaling 16 square degrees

[f] DIRBE photometric bands are 1.25, 2.2, 3.5, 4.9, 12, 25, 60, 100, 140, and 240 μm. We report the diffuse flux sensitivity rather than point source sensitivity due to the large beam size
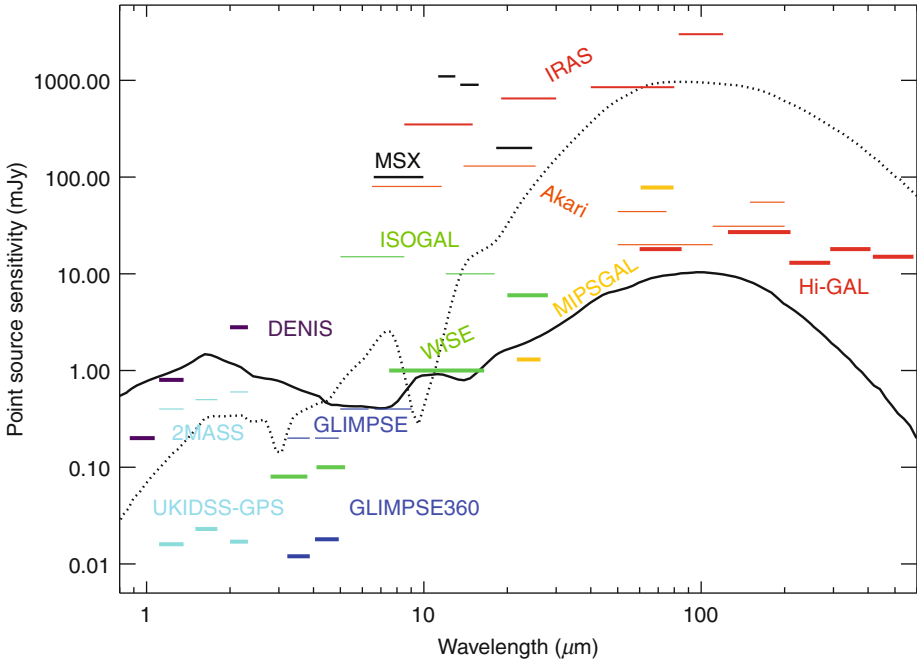
◼ Fig. 9-2

A comparison of point source sensitivities and wavelength bands of past and current ground and space-based infrared surveys. More details on these surveys are given in ❯ *Table 9-1*. The curves show model spectra of Whitney et al. (2004) for a 1 L_o T Tauri star at a distance of 0.7 kpc (*solid*) and a deeply embedded 1 L_o protostar at a distance of 0.6 kpc (*dotted*)

Among the most influential surveys were the IRAS, *Infrared Astronomical Satellite*, survey (Beichman et al. 1988; Neugebauer et al. 1984), the ISOGAL survey of the *Infrared Space Observatory* (Kessler et al. 1996; Omont et al. 2003), MSX, the *Midcourse Space Experiment* (Price et al. 2001), the all-sky COBE/DIRBE, *Cosmic Background Explorer/Diffuse Infrared Background Experiment*, survey (Boggess et al. 1992), 2MASS, *Two Micron All Sky Survey* (Skrutskie et al. 2006), DENIS, *Deep Near Infrared Survey of the Southern Sky* (Fouqué et al. 2000), *Spitzer*/GLIMPSE, *Galactic Legacy Infrared Mid-Plane Survey Extraordinaire*, (Benjamin et al. 2003; Churchwell et al. 2009), the *Spitzer*/MIPSGAL *Multiband Imaging Photometer Galactic Plane Survey* (Carey et al. 2009), and the AKARI all-sky survey (Ishihara et al. 2010).

Surveys in progress include the near-infrared surveys UKIDSS-GPS, *United Kingdom Infrared Telescope Deep Sky Survey–Galactic Plane Survey* (Lucas et al. 2008) and VVV, *Vista Variables in the Via Lactea* (Minniti et al. 2010), the mid-infrared all-sky survey WISE, *Wide-field Infrared Survey Explorer* (Wright et al. 2010) and outer Galactic plane survey GLIMPSE 360 (Whitney 2009), and the far-infrared Galactic plane survey, *Herschel*/Hi-GAL, *Hershel Infrared Galactic Plane Survey* (Molinari et al. 2010).

◨ **Table 9-2**

Effective wavelengths, zero point magnitudes, and extinction in the near- and mid-infrared[a]

Band	Wavelength(μm)	S_0	A_λ/A_K
2MASS J	1.235	1594.0	2.50 ± 0.15
2MASS H	1.662	1024.0	1.55 ± 0.08
2MASS K_s	2.159	667.0	1.0
WISE [3.4]	3.353	306.681	. . .
IRAC [3.6]	3.550	280.9	0.56 ± 0.06
IRAC [4.5]	4.493	179.7	0.43 ± 0.08
WISE [4.6]	4.603	170.663	. . .
IRAC [5.8]	5.731	115.0	0.43 ± 0.10
IRAC [8.0]	7.872	64.13	0.43 ± 0.10
MSX A	8.276	58.5	. . .
WISE [12]	11.561	29.0448	. . .
MSX C	12.126	26.5	. . .
MSX D	14.649	18.3	. . .
MSX E	21.336	8.8	. . .
WISE [22]	22.088	8.2839	. . .
MIPS [24]	23.68	7.14	. . .
MIPS [70]	71.42	0.775	. . .
MIPS [160]	155.9	0.159	. . .

[a]2MASS, IRAC, and MIPS calibration, effective wavelengths, and zero magnitude fluxes are discussed in Rieke et al. (1995) and references therein. MSX values are from Cohen et al. (2001); WISE values are from Wright et al. (2010). Typical extinctions from Indebetouw et al. (2005); see ❯ Sect. 3 information on variation with Galactic direction. For reference, $A_{[4.5]} = 0.43A_K \cong 0.05A_V$

Starting with 2MASS (near-infrared) and GLIMPSE (mid-infrared), these surveys have reached optical-quality angular resolutions and sensitivities, making it possible to detect individual stars, as well as better resolve diffuse emission and stellar clusters. This advance in resolution and sensitivity has made it possible to begin a study of the large-scale distribution of stars in the Galaxy, as opposed to the integrated light from multiple stars and diffuse dust emission. The improved angular resolution also allows for a great improvement in our understanding of massive star formation, allowing for the separation of the stars, embedded YSOs, and the complex structure of diffuse emission from PAHs and dust grains.

In this review, we discuss some of the major hallmarks of the Galaxy at infrared wavelengths. In ❯ Sect. 2, we collect and compare infrared-based results on the overall stellar structure of the Galaxy, including results from star counts and the use of standard candles. ❯ Section 3 covers the spatial distribution, extinction, and emission of interstellar dust and PAHs. In ❯ Sect. 4, we outline how infrared studies have improved our understanding of the stages and distribution of massive star formation throughout the Galaxy, leading to new methods of estimating the global star formation of the Milky Way Galaxy. In ❯ Sect. 5, we summarize some of the results of infrared investigations of evolved stars and the return of their gas and dust to the interstellar medium. We close our review in ❯ Sect. 6 with some final thoughts about the strengths and limitations of infrared investigations of the Galaxy.

The topic covered here is sufficiently vast that this review will inevitably be incomplete. Some discoveries, possibly important, will have been overlooked. Some readers may also find this review somewhat tilted to the results of the large-scale surveys, particularly in the mid-infrared (where the authors have had the most experience), as opposed to smaller area photometric and spectroscopic investigations. Finally, this review is principally focused on the Galactic thin disk and bar(s). This review will not cover infrared emission at high latitudes, e.g., the infrared cirrus or the stellar thick disk, and will only briefly touch on infrared investigations of the Galactic center region.

## 2   Stellar Content and Structure of the Galaxy

In the midplane of the Galaxy, recent infrared surveys have been detecting tens of millions of objects never before catalogued. This dramatic increase is due to three factors: greater sensitivity, improved angular resolution, and the decreased extinction at longer wavelengths (❷ *Fig. 9-3*). Depending on these limitations, as well as sky coverage, different observational programs are sensitive to different "components" of the Galaxy, i.e., bulge, disk, bar, etc. Understanding the observational limitations of these different programs, and the models used to interpret them, is vital to make sense of the disparate measurements of Galactic parameters. The section below discusses some general considerations in sorting through the zoo of available surveys, and then a review of some of the recent work in characterizing the Galactic structure.

2.1   An Overview of Infrared Galactic Stellar Surveys

Optical surveys of the Galaxy, c.f. SEGUE, *Sloan Extension for Galactic Understanding and Exploration* (Yanny et al. 2009), typically detect sources to much fainter magnitudes than current infrared surveys. However, because of the fundamental limit imposed by extinction, optical studies principally constrain the structure of the stellar halo, satellites, and the thick disk. The stellar structure of the thin disk can only be probed in the solar neighborhood, $D < 2\,\mathrm{kpc}$ (Jurić et al. 2008), and optical studies of the bulge or bar are limited to a few low extinction windows a few degrees off the midplane. Surprisingly, where deep optical studies cross the midplane, they can detect many nearby dwarf stars that are *not* seen in infrared surveys. Since infrared surveys have much lower extinction, these faint nearby dwarf stars can be lost against the brighter glare of all the more distant giant stars made detectable by lowered extinction. The effective depth (faint magnitude limit) of infrared surveys can be determined by this *confusion limit*, not just the survey *sensitivity limit*. The confusion limit depends on the angular resolution, extinction, and source density, and is a particular concern in the inner galactic plane, bar, and stellar clusters.

Current infrared surveys of the Galactic midplane are principally surveys of different classes of red giants. This can be seen in ❷ *Fig. 9-4*, which shows a TRILEGAL, *TRIdimensional modeL of thE GALaxy*,[1] simulation (Girardi et al. 2005) in the inner galaxy. One sees a decrease in the luminosity function at an absolute magnitude of $M_K \sim -1$, the break between giant and

---

[1]Girardi et al. (2005) note this word also means "very nice" in southern Brazil. And you thought the acronym GLIMPSE was contrived!
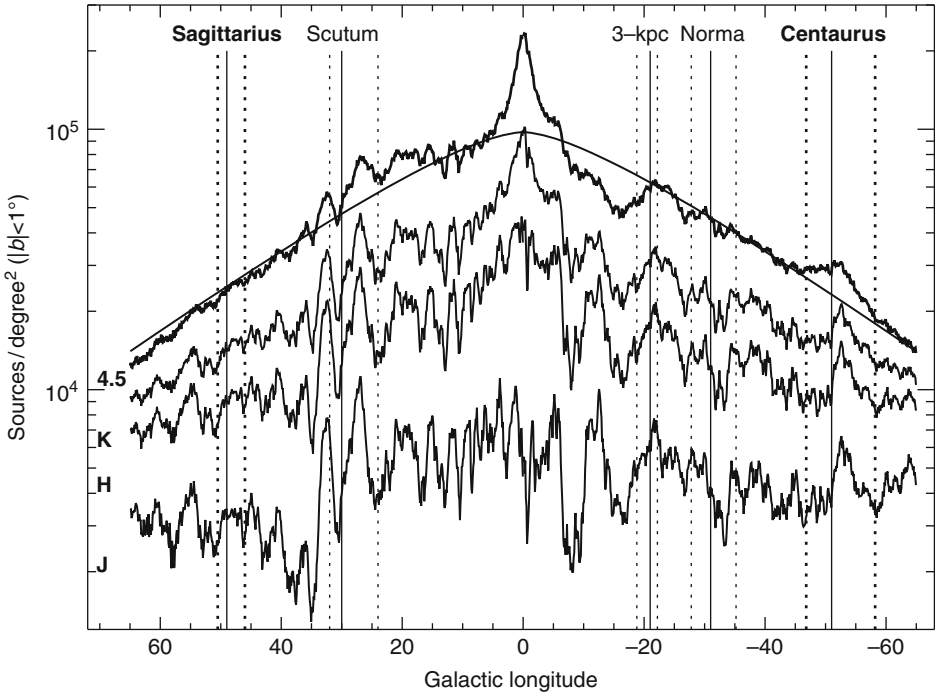
◼ Fig. 9-3

Sources per square degree in the magnitude range $m = 6 - 12$ **averaged over the latitude strip** $|b| < 1°$ **binned with a resolution of** $\Delta l = 6$ **arcminutes. The near infrared data for the J (1.2 μm), H (1.6 μm), and K (2.2 μm) bands are from the 2MASS point source catalog; the mid-infrared [4.5] band data comes from the GLIMPSE point source catalog. Note that star counts increase with increasing wavelength, and the local dips, due to clouds of absorption, become less pronounced. The fit to the mid-infrared star-count data (for** $|l| = 30–65°$ **only) is a first-order modified Bessel function of the second kind,** $N = N_0(l/l_0)K_1(l/l_0)$, **expected for an edge-on exponential disk, and yields** $l_0 = 24 \pm 4°$. **Things to note include (1) the relative symmetry between positive and negative longitudes, (2) the enhancement in source counts interior to** $|l| = 30°$ **due to the bar(s), (3) the presence of a "hole" (compared to the expectation of a filled exponential disk) from** $l = -8°$ **to** $\sim -20°$, **and (4) a broad excess centered at** $l = -52°.6$ **in the expected Centaurus spiral arm tangency direction**

dwarf stars. The confusion/sensitivity limits of $m \sim 14$ mag for recent near- and mid-infrared surveys (2MASS, GLIMPSE) mean that most of the sources detected in these surveys are giants. Current deeper surveys (UKIDSS-GPS, GLIMPSE360) should also be detecting large numbers of dwarfs in regions that are not confusion-limited.

There are two ways to convert point source catalogs into constraints on Galactic parameters: star-count models and standard candles. Surveys without sufficient angular resolution to resolve stars, e.g., COBE/DIRBE, must necessarily use the first method, convolved with the detector beam-size. The chief advantage of star-count models is that one uses all of the sources, providing excellent statistics. The chief disadvantage, discussed at length in Mihalas and Binney (1981),
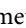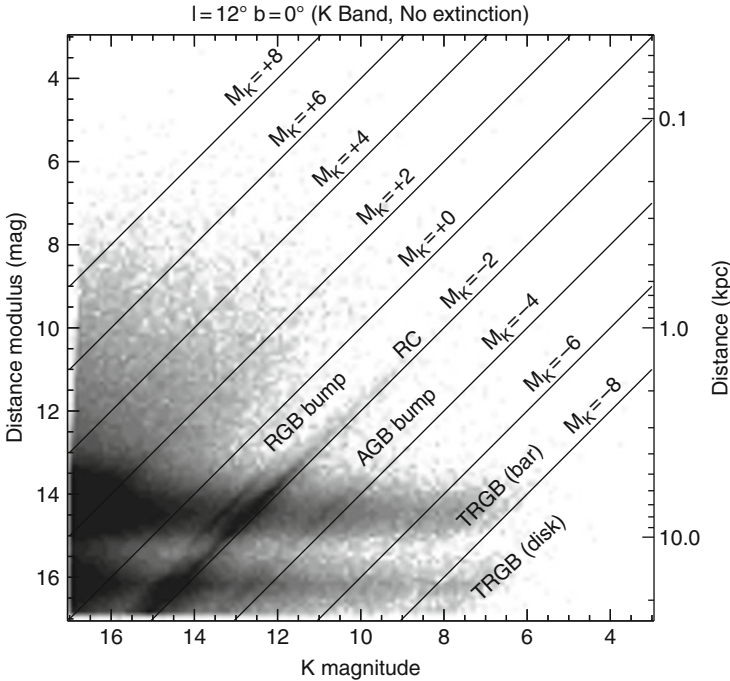
■ **Fig. 9-4**

TRILEGAL prediction for the number of sources as a function of distance modulus and predicted K band magnitude for 1 deg², zero-extinction area centered on $(l, b) = (12°, 0°)$ using the default values of Girardi et al. (2005). The horizontal band at distance modulus, $\mu = 14.5$ mag, is the contribution of the Galactic bulge (Vanhollebeke et al. 2009), while the disk contribution, which depends on the combination of space density and size of the volume element, is maximum at $\mu \sim 16$ mag. Characteristic features of the predicted giant luminosity function are noted. Lines of constant absolute magnitude are oriented diagonally. A predicted source histogram can be obtained by summing vertically along this diagram

is that extraction of Galactic parameters requires specifying (1) a model for both the stellar density as a function of position in the Galaxy and (2) the luminosity function of sources. Since the luminosity function is broad, sources at a given apparent magnitude come from a range of distances. This degrades one's ability to converge on a unique density model for the Galaxy. In addition, the resulting best-fit parameters provide a useful shorthand for summarizing results, but may be misleading in the case of unanticipated structures or degeneracies between model parameters.

There are characteristic features in the giant luminosity function (❯ *Fig. 9-4*) that can be used as standard candles to map stellar density along a line of sight. Chief among these features are the *tip of the red giant branch* (TRGB, $M_K \sim -6.85$), *red clump (RC) stars* with a local absolute magnitude of $M_K = -1.54 \pm 0.04$ (Groenewegen 2008), *red giant branch bump* stars (RGB bump, $M_K \sim -1.0$), and *asymptotic giant branch bump* stars (AGB bump, $M_K \sim -3.3$). These features have been detected in globular clusters, old open clusters, and Local Group galaxies. It is thought that the red clump star luminosity is (relatively) insensitive to metallicity or population age, with a maximum spread of about 0.4 magnitudes (Girardi and Salaris 2001). This will affect *absolute*
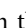
distance estimates. *Relative* distances when mapping galactic structures should be more secure unless there are large metallicity or population gradients. Other features are probably more dependent on metallicity and age effects. This can be seen in ❯ *Fig. 9-4* where the TRGB for disk stars is nearly two magnitudes brighter than the TRGB for older, metal-poor bulge stars.

Other, less common, infrared bright sources have also been used to map the inner Galaxy (principally the bars), including carbon stars (Cole and Weinberg 2002), OH/IR stars (Sevenster 1999), AGB star (Weinberg 1992), and Mira variables (Groenewegen and Blommaert 2005). A useful table describing different classes of stars can be found in Chapter 3 of Binney and Merrifield (1998). Since these sources are comparatively rare, the statistics are poorer. However, they provide important constraints on population age and metallicity that might be washed out in samples of ordinary giants. In addition, since they have a much tighter range of magnitudes, they more tightly constrain the density function of the component of the Galaxy being mapped. However, it is very important to remember that sources which trace young populations are essentially mapping the *star-forming structure* of the Galaxy, *not* the mass density.

Given the large number of potential classes of sources that can be used, one approach is to develop models that match all the features of an infrared color-magnitude diagram *simultaneously* (van Loon et al. 2003). This approach has been used with great success for Local Group dwarf galaxies. In the Galaxy, the additional free parameters needed to characterize stellar density and extinction vs position, plus the sheer volume of data to be analyzed, make this approach quite challenging.

Of the four features in the giant luminosity function discussed above, red clump stars have been put to the most use in mapping Galactic structure. This is because they have the highest space density, the tightest luminosity function, and have been absolutely calibrated using a sample with *Hipparcos* parallaxes (Alves 2000; Groenewegen 2008). Identifying red clump stars in the field is more challenging than in clusters or Local Group galaxies because of the effects of extinction and distance spreads along the line of sight. If one wants to obtain a "pure" sample of red clump giants at a given apparent magnitude, one needs color information to separate them out from brighter and fainter red giants (and dwarfs) at the same apparent magnitude.

With mid-infrared data alone, this separation is not possible. Mid-infrared wavelengths sample the Rayleigh-Jeans tail of the spectra of ordinary dwarfs and giants. As a result, the mid-infrared colors of non-dusty dwarfs and giants is near zero. However, the near-infrared colors of red clump giants is slightly bluer, $(J - K_s) = 0.70 \pm 0.05$ (Alves 2000; Grocholski and Sarajedini 2002), than most red giants, and much redder than dwarfs. They can therefore be color selected provided one can make adequate extinction corrections. The number of red clump stars per bin of apparent magnitude can be converted to mass density as a function of distance, assuming the number of red clump stars is proportional to the total mass.

There is one situation in which the distance to red clump stars can be obtained *without* color selection. Whenever there are relative overdensities in the Galaxy, a histogram of sources as a function of magnitude will have a "bump" at a magnitude related to the distance of the overdensity. ❯ *Figure 9-5* shows an example of mid-infrared histograms showing a bump at $m_{[4.5]} \sim 12.5$ due to red clump stars in the galactic "Long Bar" (Benjamin et al. 2005). If the apparent magnitude of the bump shifts smoothly with longitude, the bump is probably due a standard candle tracing a region of stellar overdensity in the Galaxy. Red clump stars are the most likely class of source to produce such a bump; near-infrared color magnitudes can be used to confirm this. ❯ *Figure 9-6* shows the slope of point source histograms as a function of longitude and magnitude for GLIMPSE 4.5 μm data. Several slope changes associated with different Galactic structures are noted and discussed below.
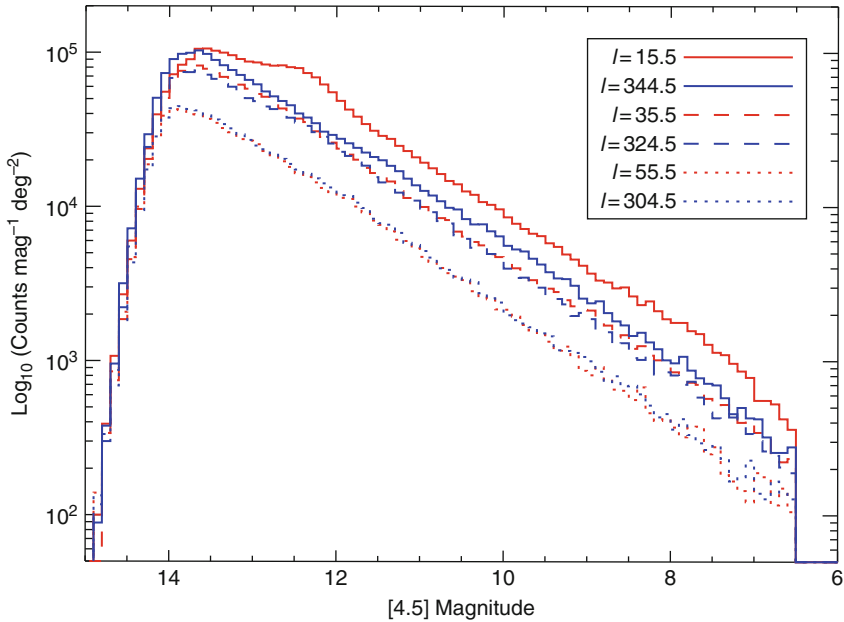
■ **Fig. 9-5**

**Number of sources from the GLIMPSE Point Source Catalog as a function of magnitude for three pairs of directions. The outer galaxy (l = 55.5°/l = 304.5°) and middle galaxy (l = 35.5°/l = 324.5°) curves have approximately the same amplitude and slopes. The inner galaxy (l = 15.5°/l = 324.5°) shows a significant north/south asymmetry; the northern direction also shows a bump in source counts at a magnitude of $m \sim 12.2$. The number of sources has been averaged over a 1° (longitude) × 1°.8 (latitude) region. Figure from Benjamin et al. (2005)**

With the rapid improvement in sensitivity and resolution, researchers are still identifying new classes of sources and developing new analysis techniques to estimate different Galactic parameters. The diversity of approaches and results can be bewildering. Which results are right? Which are suspect? This review will not make those choices. In general, the results that should carry the most weight should be those that are (1) based on all-sky (or all-plane) surveys, (2) have resolved stellar populations, (3) have the lowest intrinsic extinction, and (4) use well-calibrated standard candles.

2.2 The Stellar Disk

2.2.1 Distance to the Galactic Center

The distance to the Galactic center, R_0, is a key parameter for galactic structure. Although the official IAU value remains 8.5 kpc (Kerr and Lynden-Bell 1986), the bulk of measurements since then have favored somewhat lower values (Reid 1993). The distance to red clump stars in the bulge indicate an even smaller distance of $7.52^{\pm 0.35 (\mathrm{sys})}_{\pm 0.1 (\mathrm{stat})}$ kpc (Nishiyama et al. 2006). The two most reliable methods to get the distance to the Galactic center are infrared observations to
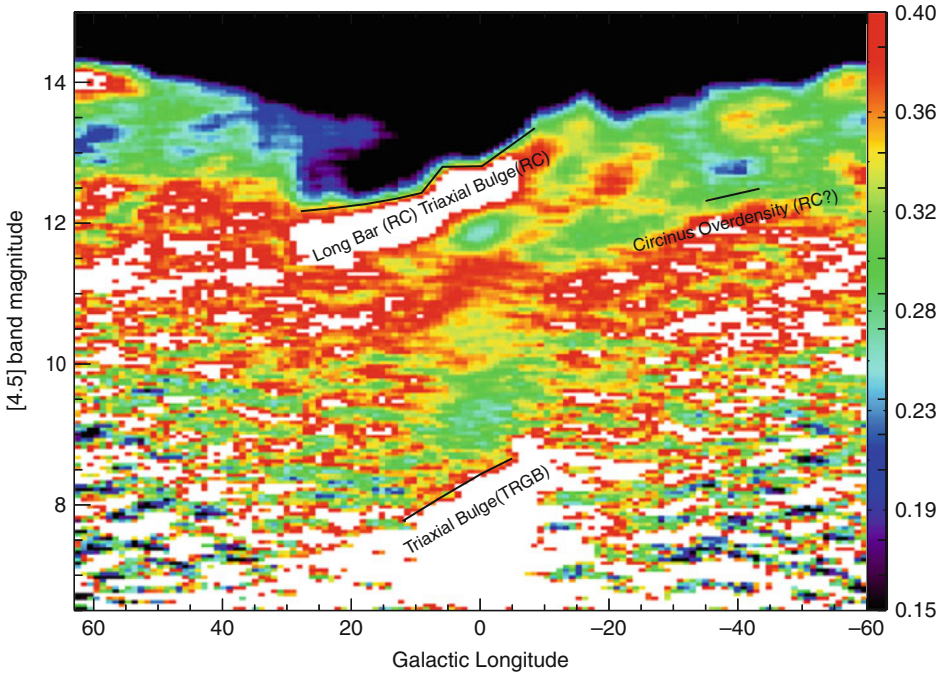
◼ Fig. 9-6

Slope of the Spitzer/GLIMPSE source histograms, log N vs magnitude, shown in ❯ *Fig. 9-5* as a function of magnitude and longitude. Color bar at the right shows the value of the slope. Density enhancements of red clump giants along a line of sight produce changes in the slope, with a magnitude that changes with longitude. Slope changes due to red clump stars in the Long Bar, the triaxial bulge, and the Circinus overdensity (possibly the Scutum-Centaurus spiral arm) are noted. The slope change in source counts in the inner galaxy around eighth magnitude is due to the tip of the red giant branch in the triaxial bulge

determine the orbital parameters of the S2 star around Sgr A*, R_0 = 8.4 ± 0.4 kpc (Ghez et al. 2008) or R_0 = 8.33 ± 0.35 kpc (Gillessen et al. 2009), and measurements of the radio parallax of the nearby Sgr B2, $R_0 = 7.9^{+0.8}_{-0.7}$ kpc (Reid et al. 2009). As observations continue for these two objects, the statistical errors will decrease. In the following sections, we have not attempted to correct reported measurements to put them on the same R_0 scale.

2.2.2 Scalelength(s)

A definitive determination of the scalelength of the Galactic stellar thin disk has yet to be made, and we are not aware of a recent critical review of the various measurements. Older studies, summarized by Robin et al. (1992b), yielded values in the range R_d = 3.5–4.5 kpc. Subsequent investigations, summarized by Sackett (1997), have usually yielded smaller values, R_d = 2.5–3.0 kpc. Since this summary, six additional optical studies have measured values ranging from 2.25 to 4.0 kpc, c.f. Jurić et al. (2008) and references therein.

Infrared studies should, in principle, give a more reliable measure of the thin disk scalelength as they can probe further through the disk in the midplane. In the inner galaxy ($|l| < 90°$), one key test of the reliability of the results is that they should be symmetric on either side of Galactic center outside the longitude range affected by the bar. In the outer galaxy, measurement of the scalelength is complicated by the presence of flaring (increase in scaleheight with radius) and warping. Results based on full-sky COBE/DRIBE low angular resolution observations of infrared light range from 2.4 to 2.6 kpc (Freudenreich 1998) and 2.3 kpc (Drimmel and Spergel 2001).

Near-infrared data from DENIS or 2MASS have also been used to constrain the scalelength, although most of these attempts have excluded the inner Galaxy. This includes analysis of DENIS data for $l = 217°$ and $l = 239°$, $R_d = 2.3 \pm 0.1$ kpc (Ruphy et al. 1996) and analysis of 2MASS data from $l = 90–270°$, $R_d = 2$ kpc (Reylé et al. 2009). López-Corredoira et al. (2002) used both star-count models and red clump giants for selected 2MASS fields in the longitude range $45° < l < 315°$ to estimate the scalelength, finding agreement between the two methods. Because the scaleheight was found to change with radius, the scalelength of the midplane density, $R_{d,0} = 2.0$ kpc, and the scalelength of the surface stellar mass density, $R_{d,tot} = 2.4$ kpc, differ. Finally, because of the reduced extinction in the mid-infrared, GLIMPSE star-count data, combined with the luminosity function of Wainscoat et al. (1992), constrained the scalelength in the *inner* Galaxy, $|l| = 30 – 65°$, yielding $R_{d,0} = 3.9 \pm 0.6$ kpc (Benjamin et al. 2005).

Making sense of all of these results would be a valuable project. As Binney and Tremaine (2008) note, given other constraints on the Galactic potential, the difference between a scalelength of 2 kpc and 3.2 kpc is the difference between a stellar mass dominated gravitational potential, and one dominated by dark matter. Some of the difficulties in comparing the results of different authors include the following: (1) observations of other disk galaxies show the radial scalelength to be wavelength dependent; (2) radial variation in the scaleheight of the thin disk and the presence of the thick disk, with a separate scalelength and scaleheight, produces potential degeneracies; (3) other galaxies show evidence of two separate scalelengths for the outer disk, depending on Hubble type (Erwin et al. 2008); and (4) surveys using photometric distances to sources need to account for binary stars (Jurić et al. 2008).

2.2.3   Spiral Structure

Spiral structure in disk galaxies is seen most prominently as a pattern of gas density and star formation. This pattern can be well organized in grand-design spirals or patchy in flocculent spirals. But disk galaxies also show spiral structure in the stellar mass, traced by infrared light. The morphology and amplitudes of the mass spiral and the star-formation spiral can be notably different (Schweizer 1976; Zwicky 1955), although they bear some similarities. The difference in arm morphology as a function of tracer is discussed at length in Chapter 6 of Binney and Tremaine (2008), who suggest the names *mass arm*, *potential arm*, *gas arm*, and *bright-star arm* to distinguish the organization of different tracers. (In this review, we refer to *star formation* arm as opposed to *bright-star arm*.) In general, the mass distribution, which is traced by the near- and mid-infrared light, is smoother and less structured than the distribution of gas or star formation, which is traced by blue light. It is even possible for the number of spiral arms seen in mass to differ from the number of arms seen in star formation (Block et al. 2004; Block and Wainscoat 1991). The idea that a two-armed mass spiral could drive more than two star

formation arms was first suggested by Shu et al. (1973); recent models intended to be applicable to the Milky Way are presented in Martos et al. (2004).

Determining the spiral structure of the Galaxy using tracers of gas and star formation has been a challenging problem (Liszt 1985) due to uncertainties in kinematic distances to gas clouds and HII regions and the uncertainties in photometric distances to the bright stars in the arms. One would expect that the spiral arm tangency directions would be more secure, but unambiguous identification of even these directions has been problematic (❷ *Fig. 9-7*). The common picture of four primary arms, *Norma*, *Sagittarius-Carina*, *Scutum-Crux*,[2] and *Perseus*, characterized by HII regions (Georgelin and Georgelin 1976), has come to dominate the literature, with other structures relegated to secondary status. These secondary features include the *Near Three Kiloparsec* arm (van Woerden et al. 1957), the *Far Three Kiloparsec Arm* (Dame and Thaddeus 2008), the *Orion Spur*[3] (Morgan et al. 1953), the *Outer Arm*[4] (Westerhout 1957), and the *Distant Arm* (McClure-Griffiths et al. 2004). The distinction between primary and secondary features is based on the number of bright HII regions thought to lie in each structure; a reexamination of this with modern data would be very informative. There is, unfortunately, no recent critical review of spiral structure in the Milky Way; we feel the current picture should still be considered provisional. ❷ *Figure 9-8* shows an artist's schematic of the Galaxy which contains most of these features at approximately the correct longitudes and estimated distances.

The spiral structure of the mass distribution of the Galaxy may be simpler. Based on near-infrared studies, mass arms are enhanced by 0.2–0.6 with respect to the azimuthal average (Rix and Zaritsky 1995) and typical cross sections (width at a given circular radius) of 20–40° (Seigar and James 1998). These widths are narrower than would be expected for a simple sinusoidal density variation, which would predict a FWHM of 60° for a two-armed spiral. This discrepancy may indicate either (1) a deficiency in the single-mode model of spiral structure or (2) indicate that the near-infrared light distribution may be affected by star formation (Rhoads 1998) as well as mass distribution.

An analysis of the K band light distribution of COBE/DIRBE suggests that Galactic spiral structure stellar mass is qualitatively different from the gas and star formation picture described above (Drimmel 2000; Drimmel and Spergel 2001). The principal evidence for this is the detection of an enhancement in near-infrared light in the direction of the Centaurus tangency, but no corresponding enhancement in the $l \sim 50°$ direction of the Sagittarius Arm tangency. This observational result is confirmed with mid-infrared star counts (Benjamin et al. 2005), which show an ~30% enhancement in star counts (of all magnitudes) centered at $l = 307°$ with a full-width at half-max of 4°. Models by Drimmel and Spergel (2001) using COBE/DIRBE near-infrared light to constrain the stellar mass distribution and the far-infrared light to constrain the dust distribution found that the data were consistent with two principal mass arms (Perseus and Scutum-Crux) and four arms in gas/star formation. The newest infrared surveys may allow for the direct *mapping* of the mass arms using red clump giants or other standard candles. ❷ *Figure 9-6* shows evidence of an enhancement in mid-infrared star counts at $l = 316$–$326°$ and $m_{[4.5]} \sim 12.3$; this longitude range is in a gap in the CO distribution (Dame et al. 2001). If this is due to red clump giants, the feature would be (approximately) consistent with the expected distance to the Scutum-Crux arm.

---

[2] Also called *Scutum-Centaurus*
[3] Also called the *Orion Arm*, *Local Arm*, or *Cygnus Arm*
[4] Also called the *Cygnus Arm*, or in a speculative leap, the *Norma-Cygnus* arm
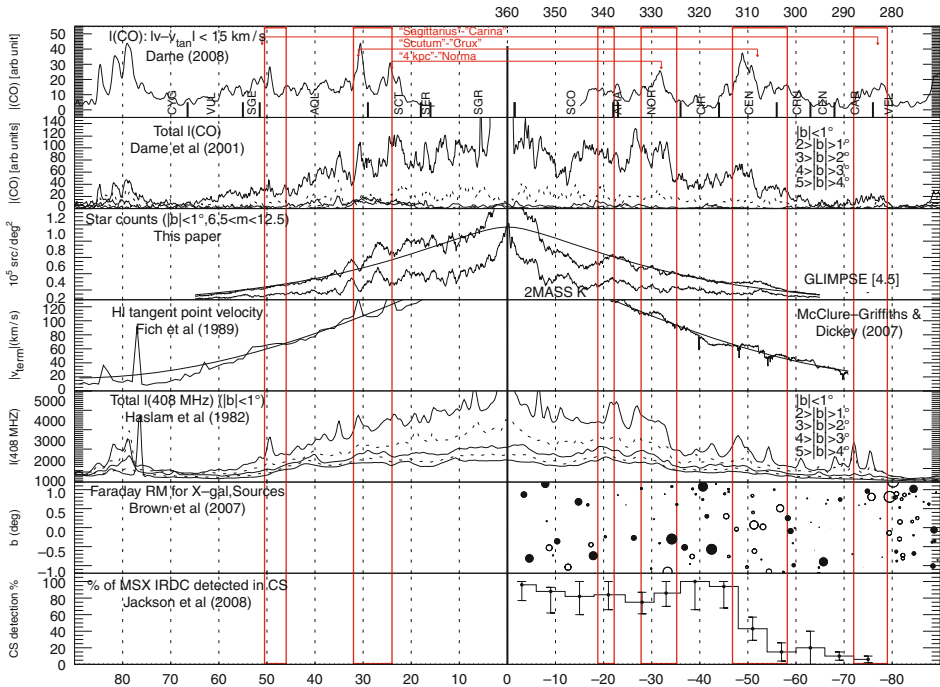
Fig. 9-7

A comparison of different tracers that might be expected to show spiral arm tangencies. From the bottom up, this includes high-density molecular clouds detected in CS (Jackson et al. 2008), Faraday rotation of extragalactic sources (Brown et al. 2007), radio synchrotron emission with different latitude cuts (Haslam et al. 1982), variations in the tangent point velocity measured in HI (Fich et al. 1989; McClure-Griffiths and Dickey 2007), mid- and near-infrared star counts (Benjamin et al. 2005), total CO intensity with different latitude cuts (Dame et al. 2001), and the integrated CO intensity within 15 km/s of the tangent point velocity. The longitude ranges for the expected tangency directions are shown and paired together for each spiral arm. Except for the top plot, there does not appear to be a compelling correlation between the data and expected tangency directions. However, the Centaurus tangency direction does appear to contain an enhancement in CO, stars, a reversal in Faraday rotation measure, and marks a significant drop in the number of infrared dark clouds that contain CS

2.2.4 The Stellar Warp, Flare, and Cutoff

An interesting and unsolved question is how to measure (or even define) the edge of galactic disks. In the Galaxy, it is not yet clear which component of the galactic disk extends to the greatest distance, the interstellar gas or the stars. What is clear, however, is that both components of the Galaxy flare (increasing vertical scaleheight with radius) and warp (changing midplane with azimuth). Evidence of the stellar warp from COBE/DIRBE data (Freudenreich et al. 1994; Freudenreich 1998; Drimmel and Spergel 2001) showed that the parameters characterizing the stellar warp were similar in phase to the gaseous (neutral hydrogen) warp (Burton et al. 1992), but smaller in amplitude. More recent attempts based on near- and mid-infrared star counts
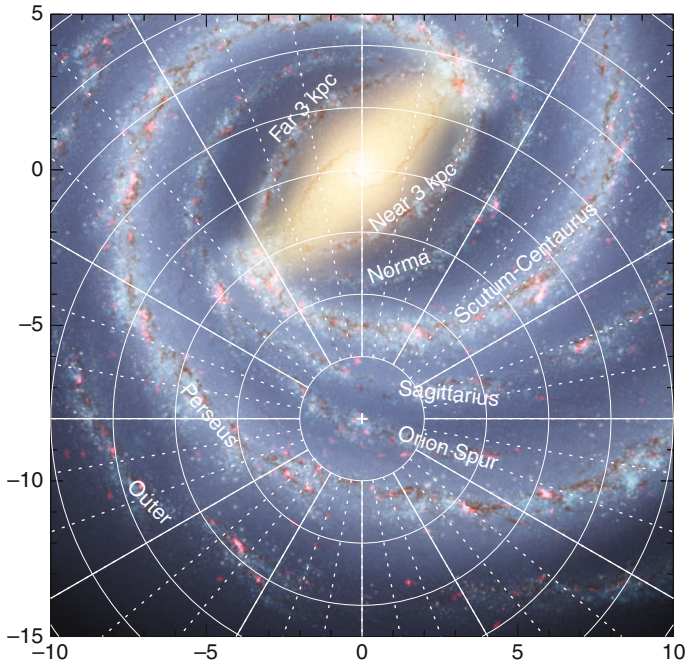
◨ Fig. 9-8

An artist's conception of the Milky Way Galaxy based on the data summarized here. Details on the construction of this image can be found in Churchwell et al. (2009). These features show most of the main structures of the Galaxy with approximately correct longitudes and distances. Circles, centered on the Sun, are located every two kiloparsecs, and Galactic longitude is marked every 10°, with l = 0° oriented upward and l = 90° to the left. Much of the structure beyond the distance of Galactic center is extremely speculative and assumes bi-symmetry

(López-Corredoira et al. 2002; Reylé et al. 2009; Vig et al. 2005) or using red clump stars as standard candles (Momany et al. 2006) have confirmed this general behavior, although there are pronounced asymmetries in the amplitude of the warp with azimuth.

The overall agreement of the gaseous and stellar warp show that the warp is due principally to gravitational as opposed to gas dynamical effects. However, the reason behind the difference in the overall amplitudes, as well as the asymmetries, is as yet unclear. Clearly, the different radial distributions of gas and stars will play a role. Extragalactic studies, e.g., Erwin et al. (2008), have found exponential outer disk profiles that are steeper or shallower than the inner disk profiles, depending on the Hubble type, although this may be a result of changes in color rather than surface density (Bakos et al. 2008). The transition point occurs around four inner-disk scalelengths, and historically had been thought to mark a disk truncation (van der Kruit and Searle 1981). Evidence for such a truncation at R = 14 kpc was reported by Robin et al. (1992a), but some of the references above detect disk stars to even greater radius.

2.3   The Galactic Bar(s)

Although gas kinematics in the inner galaxy have long been pointed to as evidence that the Galaxy has a central non-axisymmetric structure, it was not until the advent of infrared astronomy that it became possible to characterize the stellar structure of the inner Galaxy (Kent et al. 1991). Early results (Blitz and Spergel 1991) provided solid evidence of a stellar Galactic bar. COBE/DIRBE maps were then analyzed by several groups to derive constraints on the Galactic bar. The results are reviewed by Gerhard (2002) and Merrifield (2004). Most of these works tended to find a bar half-length of $R_b = 3.1$–3.5 kpc oriented in the Galactic plane at $\phi_b \sim 25°$ in the first quadrant with respect to the Galactic center direction. Published values for this angle range from $10°$ to $40°$; a partial table of values from the literature is given by Vanhollebeke et al. (2009). The bar axis ratios is 10:4:3 (length:width:height), with ranges from 10:7:4 to 10:3:3. The total stellar mass of this structure is $M_b \sim 10^{10}\ M_\odot$, with estimates ranging from $0.5 - 2 \times 10^{10}\ M_\odot$. The variations in these estimates are due to differences in the density fitting function used, the difference in luminosity functions, decisions on which other parameters (like the disk component) were held fixed or allowed to float, and incomplete sampling of the sky. The characterization of this long suspected structure, sometimes also referred to as the triaxial bulge, was one of the early highlights of Galactic infrared astronomy.

However, these studies had two disadvantages. First, the relatively poor resolution required assumptions about the unresolved stellar populations to interpret the light distribution (Dwek et al. 1995). It also made bar/bulge decomposition problematic, and meant that thin structures were poorly resolved. Second, although extinction is much lower than optical in the near infrared, it is not negligible, particularly in the midplane. As higher angular resolution infrared surveys started to yield a wealth of information about the distribution of individual types of stars across the Galaxy, the picture has become more complex. Many of these studies traced the same structure as described above. But as near- and mid-infrared surveys allowed the characterization of the stellar populations directly in the midplane, an additional structure became apparent.

2.3.1   The Long Bar

This structure, now referred to as the Long Bar, was first identified as distinct from the bulge by Hammersley et al. (2000). The dawning realization of its existence is detailed in López-Corredoira et al. (2007). Initially characterized in selected low-extinction windows in the near-infrared, the mid-infrared GLIMPSE survey showed that it could be traced continuously with red clump giants out to a longitude of $l \sim 29°.5$ (Benjamin et al. 2005). As compared to the triaxial bulge, this structure is not only longer, $R_{lb} = 3.9$ kpc, but thinner, both in vertical scaleheight, ~200 pc, and depth along the line of sight, ~1,170 pc. The estimated mass of this component, assuming it is symmetric and independent of the central triaxial bulge, is $M_{lb} = 0.6 \times 10^9\ M_\odot$ (López-Corredoira et al. 2007). Independent estimates of these parameters would be valuable.

One mystery of this structure is the distinct difference in angle for the Long Bar and the (other) Bar. This difference is not due to different measurement methods. Using red clump giant stars and UKIDSS-GPS data (also see ❯ *Fig. 9-6*), the same technique shows that the measured bar angle changes from $\phi_{lb} = 42 \pm 2°$ in the longitude range $l = 12 - 30°$ to $\phi_b = 24 \pm 2°$ for $l = 5 - 12°$. At the transition point, the star counts and number of red clump giants jump

sharply; as a result, it is not entirely clear whether the Long Bar continues to exist as a discrete structure inside $l = 12°$. Although other galaxies show evidence of multiple misaligned bars, it is not known how many of these cases are similar to that inferred for the Galaxy.

The significance of the Long Bar is in the realization that a non-axisymmetric mass distribution of the Galaxy extends further from the Galactic center than generally realized. In particular, the near end of the Long Bar coincides with the Scutum spiral arm tangency, a fact first noted by Weinberg (1992). In CO longitude-velocity plots, this direction also marks the first-quadrant tangency point of the Molecular Ring (Dame et al. 2001; Jackson et al. 2006). This intersection appears to be the site of prodigious amounts of star formation, including three large-scale height, $b = 10 − 20°$, superbubbles, c.f. Pidopryhora et al. (2007). Follow-up spectroscopy of the brightest member of GLIMPSE-identified clusters (Mercer et al. 2005) have revealed several clusters of red supergiants, c.f. Clark et al. (2009), one of which is estimated to have a total mass of $20,000 M_\odot$ (Alexander et al. 2009). There is also tentative evidence for star formation at the far end of the Long Bar at $l \sim 345°$ (López-Corredoira et al. 2001; Sevenster 1999). This deserves further scrutiny.

The discovery of the Long Bar also points out a fundamental weakness of parametric modeling of Galactic structure. As numerical simulations of bars show, bars are not monolithic structures, but complex families of stellar orbits whose properties evolve over time. By forcing Galactic models to fit a single parameterized model (based on observations of bars in distant galaxies), we destroy information on the structural complexity of bars. Numerical simulations that start with bars as vertically thin structures eventually produce a thick inner distribution, similar to what is observed in the Galaxy (Athanassoula 2007; Debattista and Shen 2007). It is not clear whether these models can also reproduce the apparent mismatch in angles.

One way to separate the different bar components as well as test for the presence, and star formation history, of a classical or pseudobulge (Kormendy and Kennicutt 2004) is to obtain information on the kinematics and metallicity of individual stars. We do not review the status of these efforts due to lack of space and expertise on the part of the reviewers. A good starting point would be the papers by Zoccali (2010) and Babusiaux et al. (2010). We note, however, that much of this work has been in optical wavelengths, which may give misleading or incomplete results due to the limitations of extinction.

2.3.2 Inner Bar?

Observations of other galaxies show up to *three* nested bars (Erwin et al. 2008), so apparently there is room for one more bar in the Galaxy. Evidence for an inner (sometimes called nuclear) bar, or at least an inner non-axisymmetric structure, has been suggested by the noncircular orbits of gas in the inner few degrees of the Galaxy (Binney et al. 1991), extinction-corrected 2MASS star counts (Alard 2001), and a combination of both of the above (Rodriguez-Fernandez and Combes 2008). This final work suggests a bar mass of $M_{nb} = 0.2 \times 10^{10}\ M_\odot$ and a bar angle, based on the kinematic modeling, of $\phi_{nb} = 60 − 75°$ relative to the Sun-Galactic center direction. This angle is marginally consistent with their independent estimate based on star counts. Other relevant studies that constrain this structure are Launhardt et al. (2002), van Loon et al. (2003), and Sawada et al. (2004). In addition, red clump giant mapping by Nishiyama et al. (2005) shows a flattening of the magnitude vs longitude track of red clump giants for $l = −5°$ to $+5°$. Based on

the evidence so far, it seems that an inner, $|l| < 2°$, mass asymmetry is likely, but its parameters have yet to be firmly established.

2.3.3 The Inner Hole (and Ring?)

The Milky Way is a barred spiral galaxy, but is it a *ringed* barred spiral? Many of the same references that characterized the stellar distribution of the disk and bar (and ❷ *Fig. 9-3*) require the presence of a central "hole." Strictly speaking, this is a deficit in stellar density compared to an extrapolation of the exponential disk into the center of the Galaxy. The hole radius is typically 2.7–3.3 kpc with an ellipticity of 0.8–0.9, e.g., Freudenreich (1998). Many barred galaxies are found to have central holes (Ohta et al. 1990); such galaxies are also referred to as Freeman Type II disks (Freeman 1970). A depression in the stellar density inside the radius of the bar is a natural consequence of bar formation, but so far as we know, there has been no detailed comparison between the current dynamical models and the Galactic data constraining the properties of the bar *and* "hole."

Whether the Galaxy contains a stellar ring, i.e., an *overdensity* of stars surrounding the bar, is considerably more uncertain. There is no compelling evidence for a stellar ring in the *mass* distribution, although obtaining constraints on the ring is complicated by the presence of the bar in the same longitude range. However, there are two structures that could arguably be identified as an interstellar, star-forming ring. The first is the "Molecular Ring" (Burton et al. 1975; Jackson et al. 2006; Scoville and Solomon 1975). First discovered in the first quadrant of the Galaxy, it is clear that a significant fraction of the molecular gas and star formation of the Galaxy is located in an annulus of radius 3–5 kpc. However, it is very difficult to distinguish between a spiral and ring. Several authors have expressed doubts about whether this feature should be interpreted as a ring, c.f. Binney and Merrifield (1998) or Jackson et al. (2008).

Another structure that might plausibly be visible as a star-forming ring to an outside observer is the Near/Far Three-Kiloparsec Arm (Dame and Thaddeus 2008). Simulations of gas flow in a gravitational potential consistent with the Galactic bar (Bissantz et al. 2003; Englmaier and Gerhard 1999; Fux 1999) predict that these two structures should form an oval around the bar. Although early searches of this structure showed no evidence for star formation (Lockman 1980), recent surveys of class II methanol masers show approximately 20 sources in each arm (Green et al. 2009), indicating the presence of massive star formation. An excess of OH/IR stars (Sevenster 1999) and enhanced near-infrared star counts of bright stars, $m_K < 9$ (López-Corredoira et al. 2001), have been noted at $l = 338°$. Both authors noted the coincidence of this direction with the tangency direction of the Near Three-Kiloparsec Arm and suggested that this might be part of a ring, even before the discovery of the Far 3 kpc Arm! A comprehensive model combining the constraints on the mass *and* star formation distribution of this structure, in comparison with the variety of rings seen in other barred spirals (Buta and Combes 1996), would be a worthy endeavor.

3 Interstellar Dust

The distribution and physical state of dust grains with Galactic environment is a vast topic. The most complete review can be obtained in the review by Draine (2003), the monograph by Whittet (2003), or the dust-related chapters in the textbooks of Tielens (2005) or Kwok (2007).

Here we limit our review to recent results in the near- and mid-infrared. The coming deluge of information on longer wavelength dust emission from the *Hershel and Planck* missions means that this will be a rapidly advancing field in the next several years.
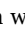
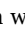## 3.1 Spatial Distribution of Extinction

The distribution of dust throughout the Galaxy, like the distribution of gas, is clumpy. Gas clouds have been traditionally mapped using kinematic distances. But given their relatively smooth distribution, stars could also serve as good tracers of the dust distribution, provided that the extinction to the stars can be reliably estimated. A succinct review of the history and current status of this approach can be found in Robin (2009). The goal is to obtain a three-dimensional map of dust clouds with the highest possible angular and distance resolution, since the extinction is known to be very patchy, and some dust clouds may be quite distant (and therefore appear small).

Drimmel et al. (2003) proposed a three-dimensional extinction model based on their parametric model of the stellar and interstellar distribution constrained by COBE/DIRBE studies. Marshall et al. (2006) assumed a smooth stellar distribution taken from the Besançon model (Robin et al. 2003) and then adjusted extinction vs distance to match the observed 2MASS color magnitude diagrams, obtaining an angular resolution of 15 arcminutes and ~100 pc in distance. López-Corredoira et al. (2002) used the distribution of color magnitude selected red clump giants to map extinction along the line of sight, a technique that was also adopted by Durant and van Kerkwijk (2006) and Stead and Hoare (2010). Each of these approaches has different assumptions regarding the background distribution of stars, and therefore can be expected to have different systematic biases. However, because of the patchy nature of the distribution, and different angular and distance resolutions, it is not straightforward to compare the different model predictions. Both Marshall et al. (2009) and Stead and Hoare (2010) compare their extinction distances to the kinematic distances, finding the two distances are correlated. However, Marshall et al. (2009) find that extinction distances in the fourth quadrant were systematically ~2 kpc more distant than kinematic distances.

In principle, extinction distances can provide a much needed check on kinematic distances, particularly for gas in the spiral arms and bars, where one might suspect that circular rotation is a poor assumption. Marshall et al. (2006) shows evidence of spiral structure in the distribution of dust clouds. Within three kiloparecs of Galactic center, Marshall et al. (2008) compare this technique with the results obtained using noncircular kinematic models of gas flow in a barred potential, showing that both techniques give the same distance to clouds that they interpret as dust lanes in the Galactic bar.

3.2 Wavelength Dependence of Extinction (Mid-infrared)

A good overview of wavelength dependence of extinction may be found in Draine (2003). Here we will only update the results obtained in the mid-infrared since that review. Lutz et al. (1996) used ISO spectral line observations to derive the diffuse interstellar extinction law using infrared hydrogen recombination lines toward the Galactic center. They found that A_λ/A_V is essentially constant from ~4 to 8 μm. Jiang et al. (2006, 2003) used ISOGAL and DENIS data toward an 0.1 deg^2 area centered at $l = 18°.6$, $b = 0°.35$ and found a similar flattening of extinction as Lutz et al. (1996). Indebetouw et al. (2005) confirmed these early results using GLIMPSE stellar photometry of red clump giants toward three other lines of sight.

Recently, both Gao et al. (2009) and Zasowski et al. (2009) have conducted a systematic study of the MIR extinction law from 1.2 to 8 μm over a large range of Galactic longitudes, and compare their results to the single-direction extinction measurements made by several groups, including those works mentioned above. The study of Zasowski et al. (2009) used about 150° of contiguous longitude at the Galactic midplane using data from 2MASS and Spitzer surveys (GLIMPSE, Vela-Carina, and Argo). They isolated a sample of red clump giants in J vs (J-K_s) color-magnitude diagrams, and determined the color excess ratios (*CER*) of this sample in (H-λ) vs (H-K_s) for the *Spitzer*/IRAC and 2MASS bands. The extinction law, A_λ/A_{K_s}, in their formulation depends only on A_H/A_{K_s} and CER_λ. They used A_H/A_{K_s} = 1.55 for all longitudes, noting this quantity is likely to be a function of Galactocentric radius. The average change in extinction with longitude from 5.8 to 8.0 μm is shown in ❯ *Fig. 9-9*. They interpret the increase of $A_{[8.0]}/A_{[5.8]}$ with longitude as evidence for a decrease in mean dust grain size toward the outer Galaxy, noting the Galactic abundance gradient may play a role as well. The grain size dependence is motivated by the theoretical dust models of Weingartner and Draine (2001), which are reproduced in ❯ *Fig. 9-9* along with the observed/derived values as a function of longitude.

In contrast, using the same data and a slightly different selection criterion for red clump giants Gao et al. (2009) found an approximately constant value of A_λ/A_{K_s} with galactic longitude, with possible deviations from this constant value in the direction of spiral arm tangencies. When they used red giants, rather than red clump giants, to measure the extinction, A_λ/A_{K_s} was systematically higher, by about ~0.05. This is presumably because red giants span a larger range of distances. Although both works find that A_λ/A_{K_s} decreases with increasing wavelength, the values found by Gao et al. (2009) are systematically higher than those found by Zasowski et al. (2009). It is not clear why one group finds a longitude dependence for the extinction law while the other group does not.

3.3 PAHs Emission

One of the most notable features of mid-infrared images of the Galactic plane is the highly structured diffuse emission. In the GLIMPSE/MIPSGAL surveys, the structure of the diffuse emission changes notably with wavelength, as the relative contributions from unresolved stellar emission, scattered starlight, atomic and molecular emission, and thermal dust emission changes. In the [3.6] and [4.5] *Spitzer*/IRAC bands (where the number is the central wavelength), much of the diffuse emission is due to unresolved point sources (particularly in the inner Galaxy), scattered starlight, and thermal dust emission (particularly in the vicinity of hot stars and regions of massive star formation). The [3.6] band also contains a polycyclic aromatic hydrocarbon (PAH) emission feature at 3.3 μm.

The diffuse emission in the [5.8] and [8.0] bands primarily traces the distribution of PAHs with minor contributions from thermal dust emission near hot stars and stochastic emission from very small dust grains (VSGs) transiently heated by UV photons. Examination of the GLIMPSE/MIPSGAL mosaic images shows that the PAH emission in these bands is widely distributed in the Galactic disk. This emission is brightest at the midplane and declines rapidly with latitude. There are also bright spikes centered on massive star formation regions, many of which are off the plane. Superimposed on the overall variation, the PAH diffuse emission is also characterized by numerous bubbles (Churchwell et al. 2007, 2006) and filamentary structures that may be the result of interstellar turbulence (Heitsch et al. 2007).
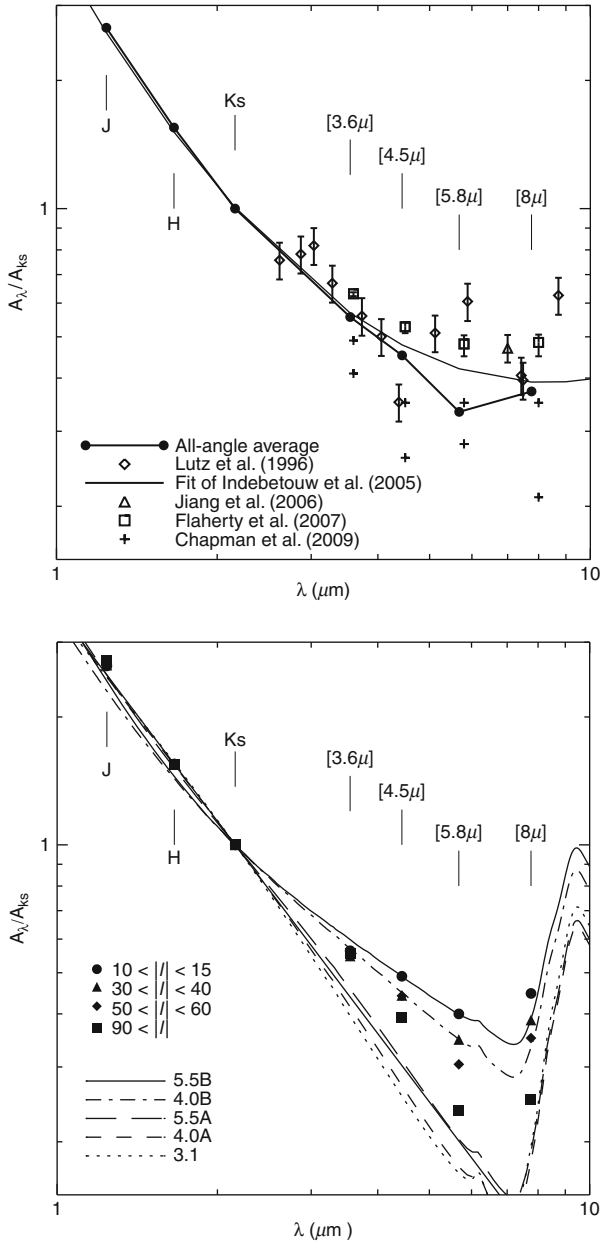
■ **Fig. 9-9**

[*Top*] **Mid-IR reddening as a function of wavelength along different lines of sight through the disk of the Galaxy from different groups noted in the figure. This figure illustrates both the differences between the different groups and the general similarity between them, in particular, the flattening from ~4.5 to 8.0 μm. [*Bottom*] The observed reddening with wavelength as a function of Galactic longitude for $10° < |l| < 90°$. Several models from Weingartner and Draine (2001) are also plotted showing a change in dust properties that might explain the observed change in the reddening law with longitude. Both figures are from Zasowski et al. (2009)**

Figure 9-10 (top) shows the diffuse emission along the Galactic midplane in a residual, i.e., point-source subtracted, [8.0] band image for different latitude cuts. With the exception of the bright spike at the Galactic center and many massive star formation region spikes, the PAH diffuse emission is almost constant, with an average value of ∼ 75 MJy/ster, within ∼ 30° of the Galactic center, falling off rapidly for $|l| > 30°$. The [8.0] diffuse emission peaks at $b = 0°$ and is tightly confined to the plane. This distribution implies that the inner Galactic plane is permeated by PAHs, whether the decline in emission with longitude traces a decrease in the PAH abundance or a change in the soft (far-ultraviolet) radiation or both is unclear. A detailed characterization of this diffuse emission has been done by Robitaille et al. (2012). A comparison of the Galactic emission with the results of PAH distribution in other galaxies (Draine et al. 2007) could be very informative.
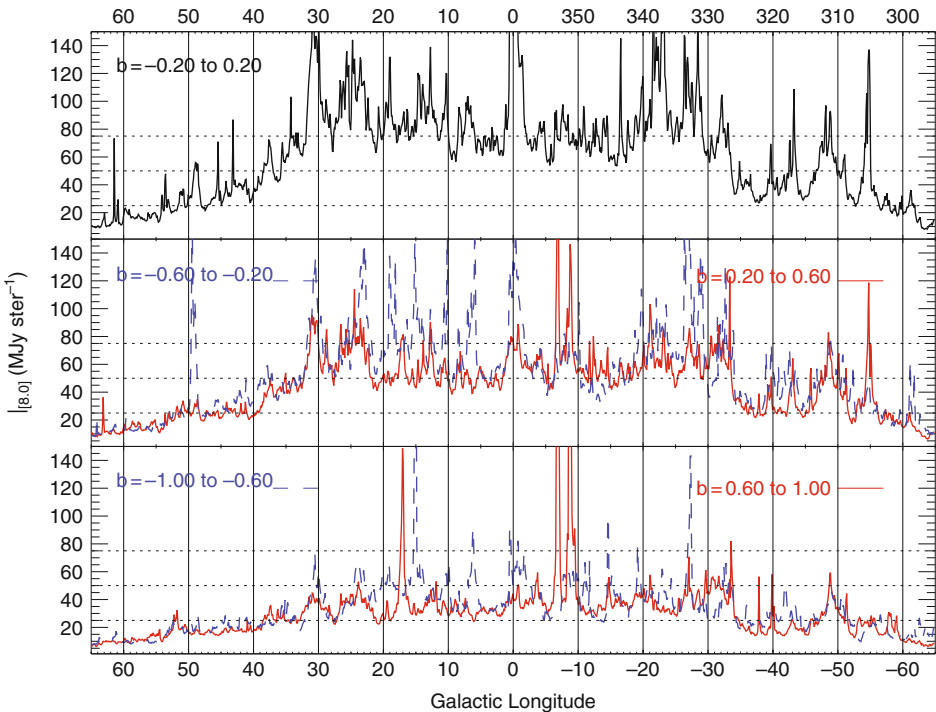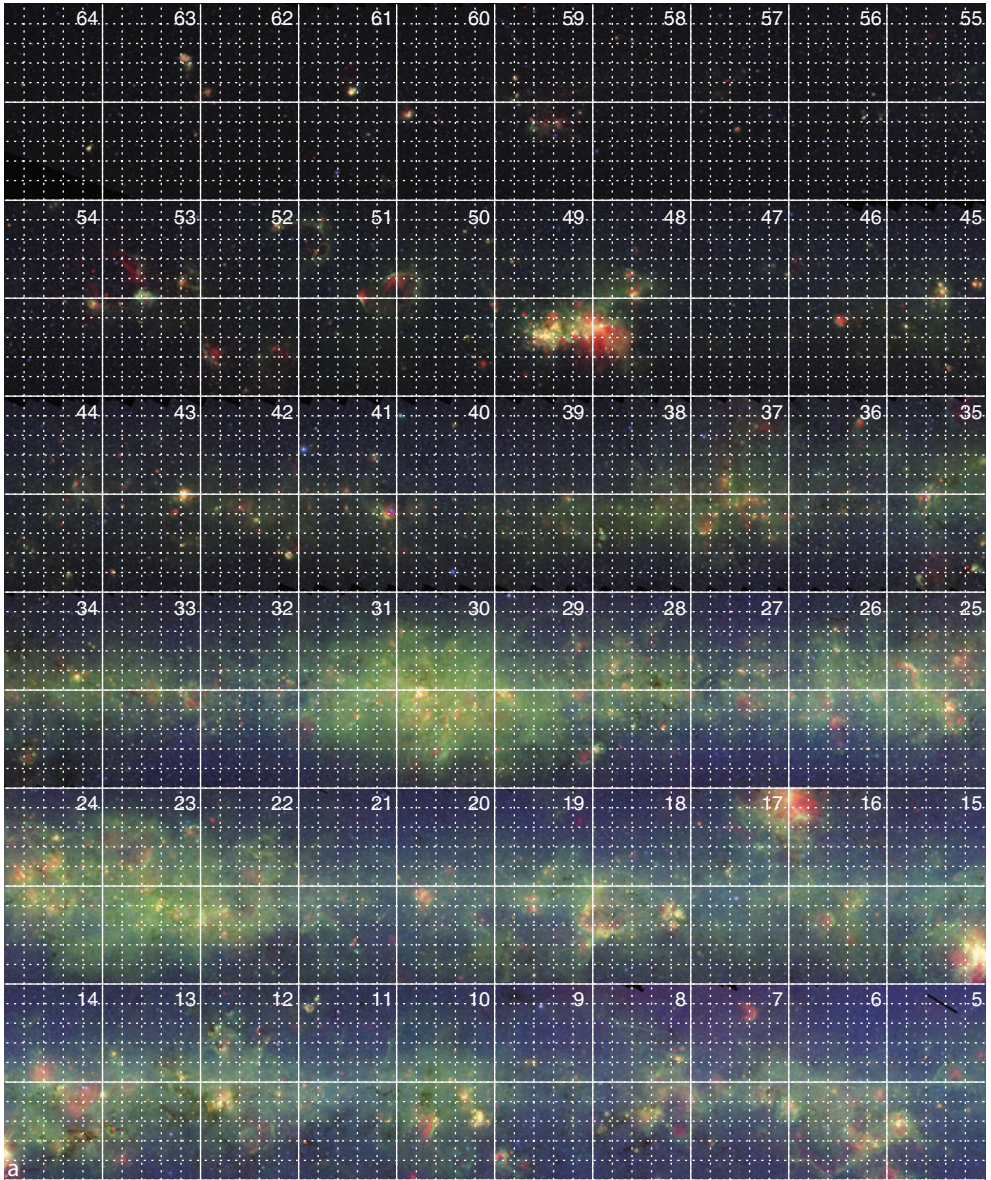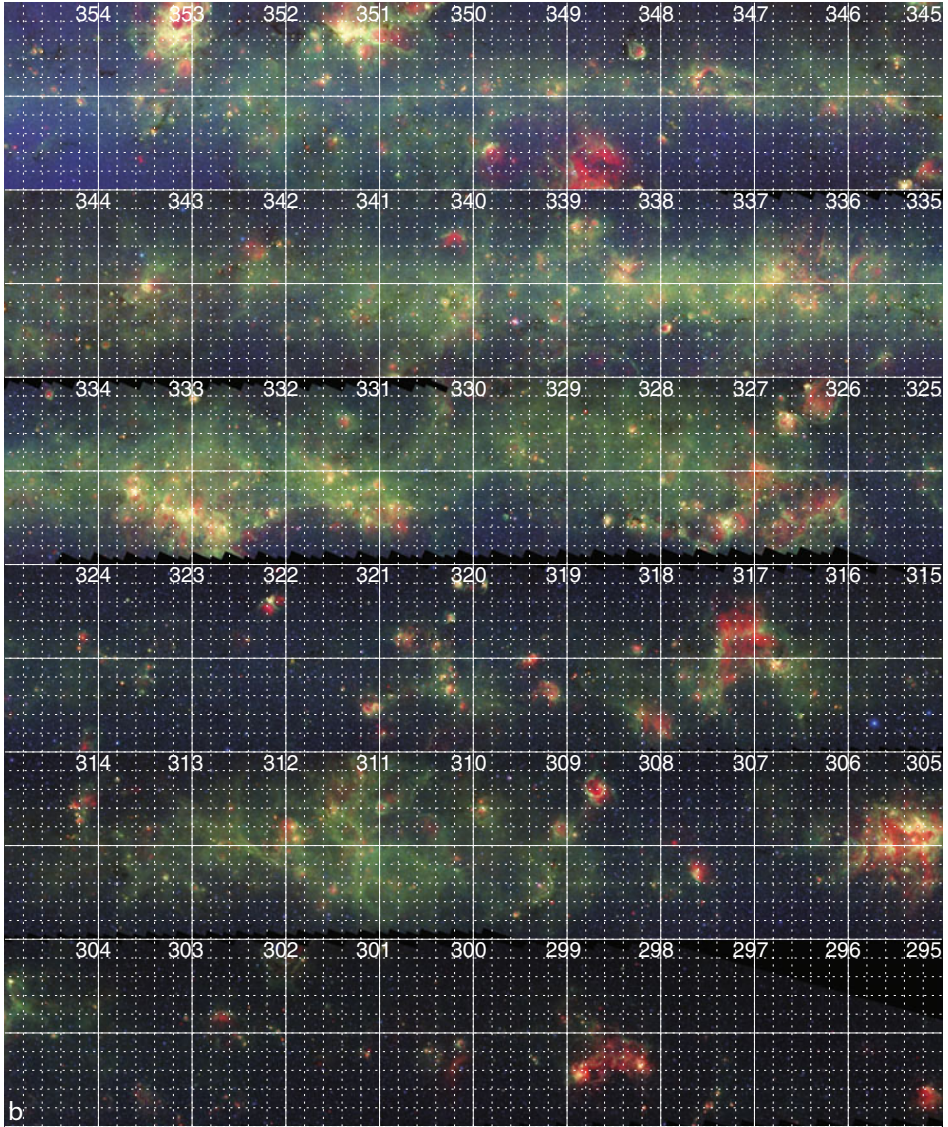

◼ **Fig. 9-10**

A profile along the Galactic plane of diffuse emission in the *Spitzer*/IRAC [8.0] band from $l = 65°$ to −65° averaged over five different latitude cuts. The diffuse emission is taken from a point-source subtracted image of the Galactic plane, smoothed to a resolution of 3′. Horizontal lines at 25, 50, and 75 MJy ster^{-1} are added to compare the drop in intensity with latitude. The lower envelope of diffuse emission interior to $|l| \lesssim 30°$ is approximately constant, but drops much more rapidly with latitude than the diffuse emission in the longitude range $|l| \gtrsim 30°$

◼ Fig. 9-11a
The GLIMPSE/MIPSGAL surveys with 4.5 μm (*blue*), 8.0 μm (*green*), and MIPS 24 μm (*red*). Hallmarks of the mid-infrared view of the Galaxy include PAH bubbles, IRDCs, YSOs, diffuse dust/PAH emission, and millions of stars. Each strip spans 10° of the Galactic plane, centered on *l* = 60° (*top* panel) down to *l* = 10° (*bottom* strip). Many of the HII regions seen in this image, characterized by (*red*) 24 μm dust emission in the inner part of the HII region and surrounded by (*green*) 8 μm PAH emission in a photodissociation region, have yet to be catalogued and classified
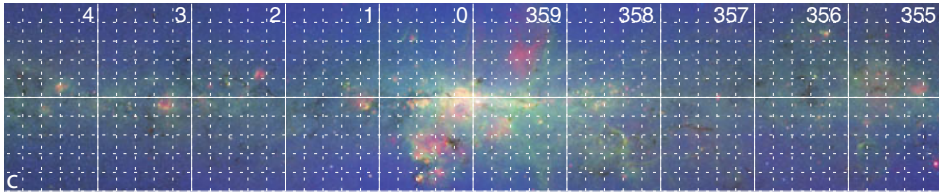
⬛ **Fig. 9-11b**

Same as ❯ *Fig. 9-11a* but for *l* = 295 – 355°. **Each strip spans 10° of the Galactic plane, centered on** *l* **= 350° (***top* **panel) down to** *l* **= 300° (***bottom* **strip)**

3.4 Stochastic and Thermal Dust Emission

The longer wavelength emission characterized by emission in the *Spitzer*/MIPSGAL [24] band is primarily due to dust heated by starlight (Draine 2003). As shown by Draine and Li (2001), the temperature of grains smaller than about 50 Å in a given interstellar radiation field (ISRF) strongly fluctuates with the absorption of single photons (which occurs on timescales $\gtrsim 1.7\,\mathrm{h}$). In contrast, grains larger than about 200 Å have essentially a constant temperature. The former

■ **Fig. 9-11c**
Same as ❯*Fig. 9-11a* but for *l* = −5° to 5°

process has been referred to as stochastic heating and the latter to thermal heating because it is in equilibrium with the radiation temperature of the ISRF. Thus, the 24 μm emission measured by the MIPSGAL survey is expected to track the integrated intensity (over all wavelengths) of the ISRF convolved with the size distribution of dust grains and their spatial distribution throughout the Galaxy.

❯ *Figure 9-11a–c* show false color images of the entire GLIMPSE/MIPSGAL survey, showing the distribution of starlight in the [4.5] band (blue), PAH emission in the [8.0] band (green), and dust emission in the [24] band. The brightest 24 μm emission shows a strikingly different morphology than the 8 μm emission. The longer wavelength emission appears to be much patchier, brightest in the regions around hot stars (young star clusters, HII regions, young stellar objects) and AGB stars. The difference in the sky distribution of the emission from PAH and small dust grains sampled by the two bands indicate spatial variations in the ISRF, the PAH-to-dust grain ratios, or both. For example, Draine (2003) estimates that between 3 and 50 μm, 40% of the integrated dust emission is emitted in the wavelength range 12–50 μm while 60% falls in the 3–12 μm range, due to PAH emission. Both the hard component ($E > 13.6$ eV) and the soft component ($E < 13.6$ eV) of the ISRF are primarily produced by hot stars (O and early B stars), but since the soft UV photons can pass through HII region ionization fronts and propagate further into the ISM from hot stars than the hard UV photons, the wider diffuse distribution of 8 μm vs the patchy 24 μm emission is a logical consequence.

4 Star Formation

Since stars form in dense and dusty environments, it had always been anticipated that the advent of infrared astronomy would lead to a major advance in our understanding of the nature and distribution of star formation throughout the Milky Way, particularly massive star formation. What may be less appreciated is how the rapidly improving angular resolution of these surveys has led to an explosion in the number of known star formation regions at greater and greater distances from the Sun. For example, a recent *Green Bank Telescope* hydrogen recombination line survey of the Galactic plane (l = −16° to 67°) that targeted 24 μm and 20 cm bright diffuse sources had a 95% success rate (Bania et al. 2010). This single effort has doubled (!) the number of confirmed Galactic HII regions in this section of the Galaxy. When these new objects are plotted on a position-velocity diagram, clear evidence is seen for structure in the star-forming component of our Galaxy, including the enhanced star formation at the near end of the Long Bar, a multi-peaked radial distribution, and star formation in the Outer Arm at a distance of over 20 kpc from the Sun.

It is not just the study of classical HII regions that is currently undergoing a renaissance. In a review of the stages of massive star formation, Churchwell (2002) noted that "the evolutionary stages preceding the ultra-compact HII region state are not well understood, and future efforts are likely to concentrate on these." Infrared surveys have fulfilled this promise, yielding catalogues of entirely new classes of objects associated with star formation, e.g., infrared dark clouds, high mass stellar outflows, massive young stellar objects, and PAH bubbles. The physical properties of these objects are now being studied; their Galactic distribution has yet to be investigated.

4.1   Infrared Dark Clouds

Infrared dark clouds (IRDCs) are the densest condensations in giant molecular clouds, the most likely sites of future star and cluster formation, and the repository of the Galaxy's densest molecular constituents. IRDCs also inform us of the conditions necessary for star formation. IRDCs were first identified in the Galactic plane from *Infrared Space Observatory*/ISOCAM images, followed closely by the detection of ~2,000 IRDCs from *Midcourse Space Experiment* images. A review of much of the work done on these clouds, both in infrared and molecular emission, can be found in the review by Churchwell et al. (2009). IRDCs are typically opaque at 8 μm, implying extinctions $A_{[8.0]} > 3$ mag ($A_V > 70$ mag). These objects are a striking feature of infrared surveys and can be mapped at very high angular resolution. However, the requirement of a bright diffuse mid-infrared background imposes a strong selection bias. In directions with low diffuse mid-infrared emission, i.e., increasing galactic latitude or longitude, clouds with the same physical properties as IRDCs would have to be identified by molecular line emission.

Studies with MSX and ISO first drew attention to the importance of these objects. The GLIMPSE survey, because of its greater sensitivity and spatial resolution than MSX, has revealed an even larger number of IRDCs and provided a more detailed picture of their morphologies, especially those clouds with small angular sizes. Peretto and Fuller (2009) released a catalog of 11,202 *Spitzer*/GLIMPSE IRDCs, 80% of which were not in the previous MSX-based infrared dark cloud catalogue (Simon et al. 2006).

Many studies of IRDC properties have been undertaken using various radio molecular probes and radio continuum observations. These investigations indicate typical densities $> 10^5$ cm^{-3}, temperatures $\lesssim 20$ K, and masses ranging from a few $M_\odot$ to $> 10^4 M_\odot$. IRDCs are generally, but not exclusively, filamentary (see ❯*Fig. 9-12*) with length-to-width ratios often well in excess of 10:1. They consist of dense condensations embedded in a lower density diffuse envelope. Ragan et al. (2009) report substructures ranging from 0.5 $M_\odot$ cores to $\leq 10^4$ $M_\odot$ clouds,[5] with an IRDC clump mass function whose slope becomes flatter than the slope of the Salpeter initial mass function (Salpeter 1955) for $M_{clump} < 40$ $M_\odot$. They suggest that this turnover may be the transition between IRDCs that produce clustered star formation and those that produce distributed star formation; further study is needed to confirm this. The same study also yielded a clump mass-radius relation $M \propto R^{2.7}$, similar to that of Williams et al. (1994).

The internal density structure of IRDC clumps and cores can be determined using mid-infrared (MIR) absorption, in addition to the standard analyses of molecular line emission or submillimeter continuum images. Abergel et al. (1998, 1996) and Bacmann et al. (1998) were the first to use extinction profiles of isolated starless cores (low-mass IRDC cores) at

---

[5]Bergin and Tafalla (2007) define *cores* as objects with masses 0.1–10 $M_\odot$ and sizes 0.01–0.1 pc, *clumps* with 10–10³ $M_\odot$ and 0.1–1 pc, and *clouds* with 10³–10⁴ $M_\odot$ and 1–10 pc.
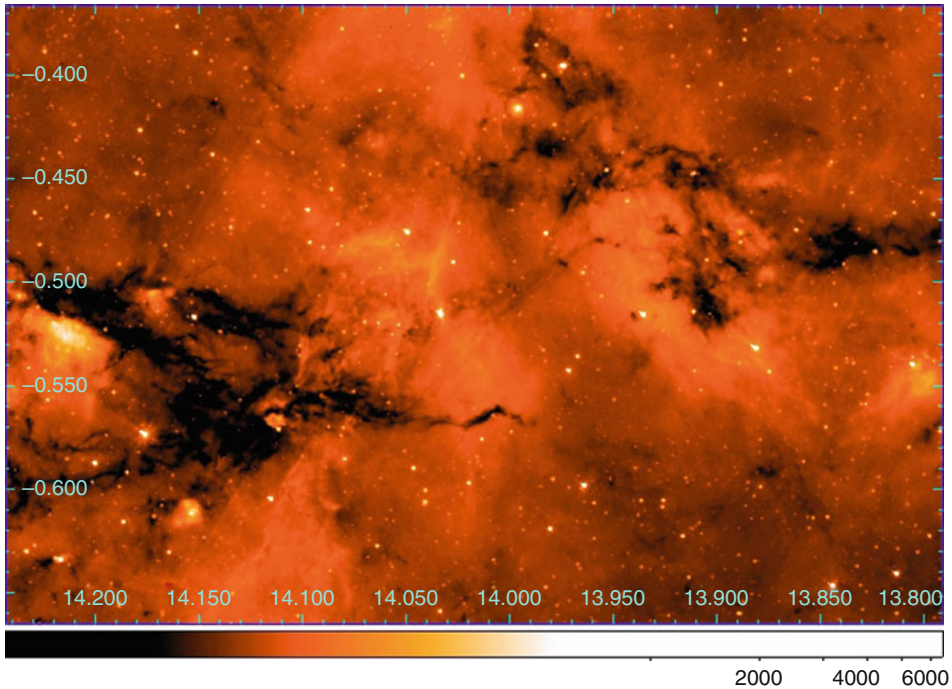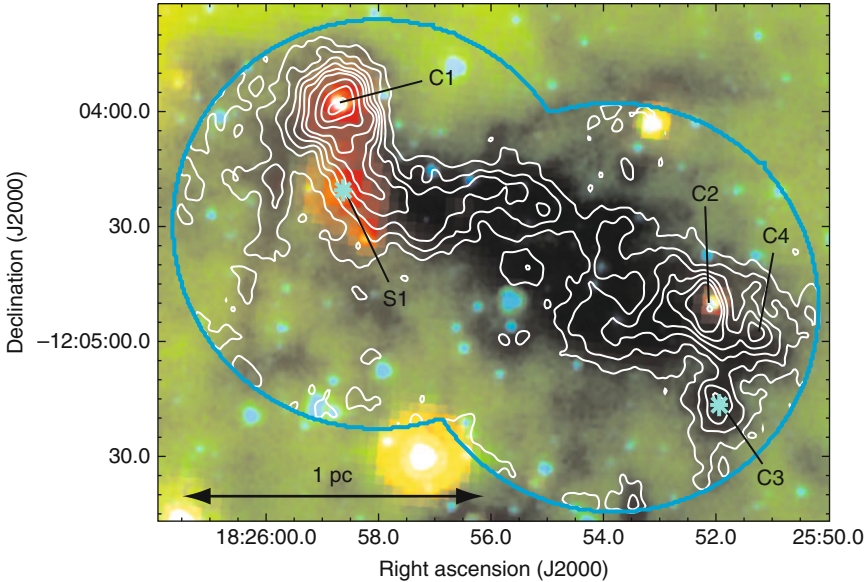
◼ Fig. 9-12
**Example of an IRDC complex in the neighborhood of M17. This illustrates how clearly IRDCs stand-
out in silhouette at 8 μm in the inner Galaxy. It also illustrates the intricate filamentry structure of
IRDCs. A closer look at this complex in a three-color image shows many probable YSOs currently
forming in this region. Figure from Devine (2009)**

MIR wavelengths to estimate the H_2 column density profiles and total masses. They found
approximately flat column density profiles out to a radius of several thousand astronomical
units. Beyond this radius, the column densities sharply decrease, confirming the earlier analy-
ses based on molecular line and submillimeter data (Andre et al. 1996; Ward-Thompson 1994).
The rapidly decreasing densities beyond the central flat region indicate that pre-stellar cores
are basically decoupled from their larger parent clouds, limiting the mass available to the core.
The significance of this is that the clump mass function, which seems to parallel the stellar mass
function but at larger masses, may depend on clump density profiles as a function of mass. This,
of course, needs further independent confirmation. Additional determinations of IRDC den-
sity profiles have been obtained for several other clouds (Andre et al. 2000; Ragan et al. 2009;
Ward-Thompson 1994).

Because IRDCs are dense, cold, and massive, one might expect them to be globally gravi-
tationally unstable, but examination of many IRDCs shows that at any given time only a small
fraction of the volume of a typical IRDC is involved in forming stars. Devine (2009) used the
VLA to obtain high resolution, sensitive images of four IRDCs in the lines of $NH_3(1,1$ and $2,2)$
and CCS (2_1-1_0). These images show that the NH_3 emission is generally optically thick ($\tau > 3$)
and closely traces [8.0] band PAH emission, with significant velocity substructures within all

Fig. 9-13

A NH$_3$ (1, 1) VLA image (contours) of the IRDC G19.30 + 0.07 (colored image from GLIMPSE/MIPSGAL (4.5 μm-*blue*, 8.0 μm-*green*, 24 μm-*red*)). The blue overlapping circles show the primary half-power beam of the VLA. The NH$_3$ emission closely follows the outline of the MIR dark cloud. Four dense and warm cores are indicated by labels C1-C4 from NH$_3$ emission, two of which are also bright 24 μm sources. The location of water masers (S1 and in C3) are shown with blue stars. C4 and S1 NH$_3$ sources do not stand out at MIR wavelengths, perhaps because they are too young to have heated dust such that it is bright at MIR wavelengths. Figure from Devine (**2009**)

four clouds. They also confirmed the general gas properties found by other investigators: densities of $\sim 10^5$ cm^{-3}, integrated masses ranging from 1,100 to 20,000 $M_\odot$, gas kinetic temperatures of 15–25 K.
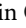
These observations also identified multiple hot molecular clumps in all IRDCs observed. An example of one IRDC with four hot NH$_3$ clumps and two H$_2$O masers is shown in ❯ *Fig. 9-13*. The NH$_3$ clumps, labeled C1-C4, appear to be in hydrostatic equilibrium. The clumps found in the other three IRDCs are thought to be collapsing because the mass of the NH$_3$ clumps is substantially larger than their virial mass inferred from line dispersions. The correspondence of some NH$_3$ clumps with bright MIR compact sources in IRDCs convincingly shows that these clumps are probably sites of current star formation in IRDCs.

4.2 Extended Green Objects

A new class of objects, discovered in the GLIMPSE survey, are now referred to as extended green objects (EGOs). These are diffuse sources that are bright in the [4.5] band (which is usually chosen as green in three- or four-color images using the *Spitzer*/IRAC bands). Cyganowski et al. (2008) visually identified and cataloged more than 300 EGOs in the GLIMPSE I survey.

These EGOs are found toward IRDCs and are frequently associated with bright 24 μm sources, indicating that they are associated with an early stage of star formation.

These sources are also strongly correlated with CH$_3$OH (methanol) masers. Class I methanol masers (44 and 95 GHz) are collisionally excited and observationally well correlated with molecular outflows in massive star formation regions (Cragg et al. 1992; Johnston et al. 1992; Kurtz et al. 2004; Plambeck and Menten 1990), while Class II methanol masers (6.7 GHz) are radiatively pumped by IR emission from warm dust, c.f. Cragg et al. (2005) and references therein, and are exclusively associated with massive young stellar objects (Minier et al. 2003). Cyganowski et al. (2009) examined the association of EGOs with methanol masers at high spatial resolution using the VLA, finding that $\geq$ 64% of the EGOs targeted were detected as Class II 6.7 GHz methanol masers. This maser transition is spatially concentrated ($\leq$ 1″) in compact groups coincident with the center of the EGOs and 24 μm emission.

In addition, ~ 90% of the observed EGOs were also detected as Class I 44 GHz methanol masers. This emission, unlike the 6.7 GHz transition, is widely distributed over tens of arcsecs and coincides with the extended [4.5] band emission, which would be expected if this emission traces molecular outflows. The methanol emission lines are broad (typically $\geq$ 20 km s^{-1}), also consistent with outflows. The James Clerk Maxwell Telescope was also used to survey these sources in emission lines of HCO$^+$ (3-2) and SiO (5-4). The detection of SiO (5-4) in 90% of surveyed EGOs is consistent with ages ~ 10^4 years or less since SiO persists for only this long after the passage of a shock. Finally, the detection of 83% of surveyed EGOs in thermal CH$_3$OH ($5_{2,3}$ − $4_{1,3}$) emission indicates the presence of warm, dense gas. Some of these results are illustrated in ❯ *Fig. 9-14* taken from Cyganowski et al. (2009).

This work indicates that EGOs are rapidly accreting massive protostars in an early stage of formation prior to the development of hypercompact HII regions. Spectra of a few of these sources (De Buizer and Vacca 2010) indicate that the emission seen in the [4.5] band is shocked molecular hydrogen, presumably created when bipolar outflows crash into the ambient ISM. If this is generally true, mid-infrared surveys provide a very easy and quick way to identify a very early and rare stage of massive star evolution.

4.3 Massive Young Stellar Objects and the Galactic Star Formation Rate

The current census of massive stars in the Galaxy is woefully incomplete. Foreground extinction obscures many of these stars in optical and near-infrared surveys, and the youngest of these sources are still surrounded by their natal molecular and dust cocoons. Happily, mid-infrared surveys have reached the sensitivity and angular resolution that the most massive stars in the Galactic disk have mostly been *detected*. The new challenge is in *identifying* which sources, out of the hundreds of millions of objects, are the massive stars and protostars.

Since the mid-IR colors of naked OB stars are indistinguished, the identification of these sources relies on the proximity of nearby dust. For massive stars that have had time to create HII regions, diffuse 24 μm emission from the dusty HII regions provides a reliable signpost (Bania et al. 2010). But mid-infrared surveys are also making it possible to find massive stars at an even earlier stage of evolution. Since these massive young stellar objects (MYSOs) are still deeply embedded in their parent clouds, the large dust envelope surrounding these protostars reemits the stellar radiation at MIR wavelengths. This makes them especially bright in the 24 μm and [8.0] bands observed by *Spitzer*.
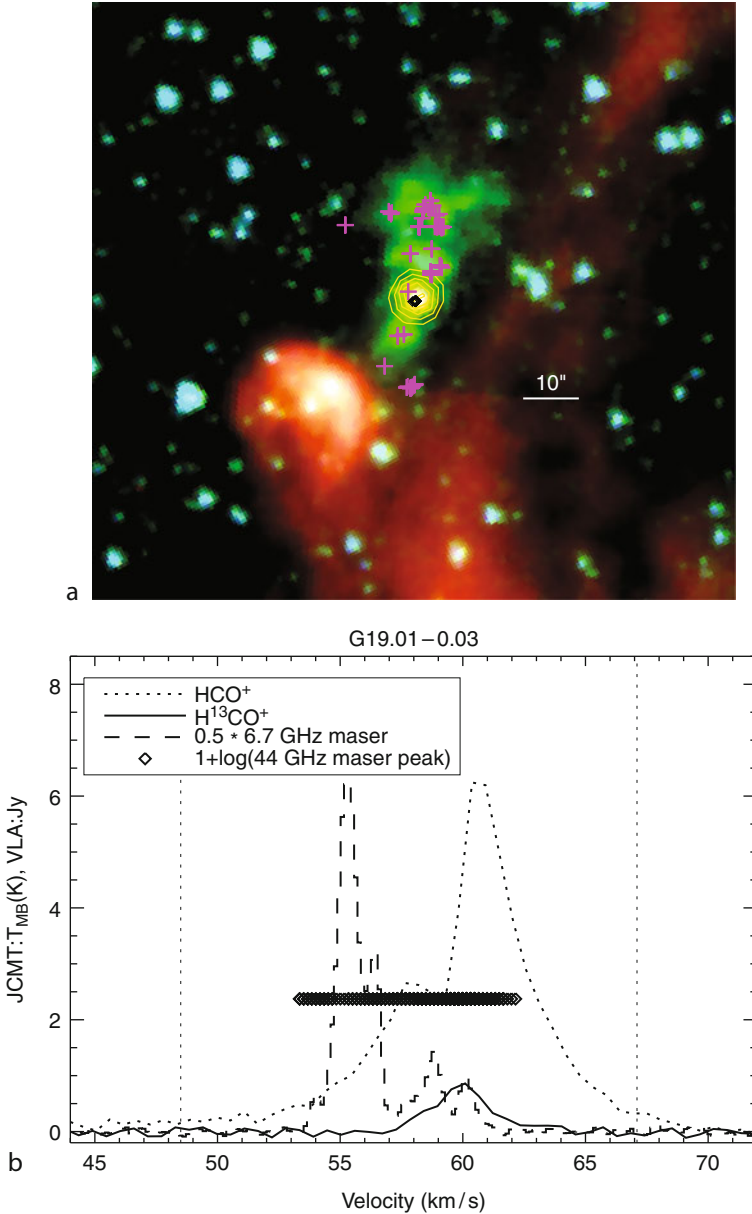
□ Fig. 9-14
(**a**) **A GLIMPSE/MIPSGAL image ([3.6]-*blue*, [4.5]-*green*, [8.0]-*red*, yellow contours-24 μm) toward the EGO G19.01-0.03. The pink and black pluses and diamond symbols represent the locations of CH3OH 44 GHz and 6.7 GHz masers, respectively. Note the extended 4.5 μm emission and the spatial distribution of the 44 GHz CH$_3$OH as opposed to the central location of the 6.7 GHz maser and 24 μm dust emission. (b) The corresponding velocity range and line profiles of the CH$_3$OH masers (6.7 and 44 GHz), HCO+, and H^{13}CO$^+$ toward the EGO G19.01-0.03. Note the broad, self-absorbed HCO$^+$ profile, the multiple, broad-velocity components of the 6.7 and 44 GHz masers. Both images are from Cyganowski et al. (2009)**

A search for these objects was undertaken by Robitaille et al. (2008) who identified over 22,000 sources in the GLIMPSE I and II surveys with red mid-infrared colors, $[4.5] - [8.0] \geq 1$. Further checks on the quality of the flux densities led to a final sample of 18,949 sources. This sample is incomplete as it does not include saturated sources, sources below the sensitivity and confusion limits, and (presumably nearby) extended sources which are not included in the GLIMPSE point source catalogs. Using a combination of color-magnitude, color-color, SED, and Galactic distribution analyses of the sample of almost 19,000 intrinsically red sources, it was found that about 40% were AGB star candidates (see ❷ Sect. 5.2) and about 60% were MYSO candidates. Planetary nebulae and background galaxies together represented ≤2–3% of the sample. Since the GLIMPSE II sample was obtained at two different epochs separated by at least 6 months, it was also possible to analyze these data for variability. About 22% of the sample was found to be variable by ≥0.3 mag in the [4.5] or [8.0] bands; these are likely AGB long period variables.

The identification of these massive stars in the process of formation allows for an estimate of the current star formation rate of the Galaxy. The global star formation rate (SFR) of a galaxy is a measure of its reservoir of cold, neutral gas. As a galaxy ages and its reservoir of gas is presumably depleted by trapping mass in burned out stars, its ability to create new stars also declines. The global SFR of a galaxy has implications for all the properties that determine the observed properties of a galaxy such as its integrated colors, stellar population, radiation field, and possibly even its dynamics. Robitaille and Whitney (2010) used an ensemble of YSO spectral energy distributions (Robitaille et al. 2007b) combined with a model of their spatial distribution to simulate the MYSO population detectable by GLIMPSE until it was in agreement with the observed MYSOs in the GLIMPSE catalog. They derived a global Galactic star formation rate in the range 0.7–1.5 $M_\odot$ yr^{-1}.

This value is significantly lower than most previous estimates of the Galactic star formation rate, which are based on indirect measures of O and B stars in conjunction with an initial mass function (IMF) to extrapolate to all masses. Smith et al. (1978) found 5 $M_\odot$ yr^{-1} based on radio free-free emission from the Galactic disk. Diehl et al. (2006) found 4 $M_\odot$ yr^{-1} from the amount of ^{26}Al in the Galaxy from γ-ray flux. Misiriotis et al. (2006) found 2.7 $M_\odot$ yr^{-1} using the IRAS 100 μm flux and a conversion factor used for other galaxies. Murray and Rahman (2010) found 1.3 $M_\odot$ yr^{-1} from the total free-free emission observed by WMAP. Surprisingly, there is no review of the global star formation rate of the Galaxy that critically evaluates and compares these results.

4.3.1 PAH Bubbles and Triggered Star Formation

Bubbles are produced in the interstellar medium by the momentum and energy input from stars and stellar clusters. They are produced by asymptotic giant branch stars, planetary nebulae, supernova remnants, HII regions, and massive young stellar objects. The high angular resolution and sensitivity afforded by *Spitzer* has led to the discovery of thousands of such bubbles. Bubbles associated with stars near the end of their lifetime are discussed in ❷ Sect. 5; here we summarize bubbles associated with star formation.

The most spectacular objects in the Galaxy at mid-infrared wavelengths are bubbles of diffuse emission, particularly in the [5.8] and [8.0] bands (Churchwell et al. 2007, 2006). The most luminous bubbles surround radio HII regions, presumably powered by radiation and winds from O and early B stars. About 38% of the MIR bubbles catalogued are incomplete rings and

appear to be "blown out" where the confining shell is thinnest. The bubbles have eccentricities between 0.55 and 0.85 with a peak at ~0.65 and are thin relative to the bubble radii. They are tightly confined to the Galactic plane with a scale height of $0.°63 \pm 0.°03$ (similar to that of O and B stars) and have average surface densities of ~ 5 deg^{-2} for $|l| < 10°$ and ≥ 1.5 deg^{-2} for $|l| > 10°$.

Multiwavelength observations of these bubbles have led to new insights on the role of dust and PAHs in HII regions (Povich et al. 2007; Watson et al. 2008). The 8 μm (PAH) emission is confined to a shell that traces the photodissociation region (PDR) surrounding the HII region. The lack of 8 μm emission interior to this shell indicates that PAHs are destroyed by the stellar UV radiation. Inside the shell, the mid-infrared bubble is characterized by thermal dust emission, especially at 24 μm. In some cases, there is also an 8 μm emission peak at the location of the central star, although this is probably thermal dust emission and not PAHs. Radio continuum and 24 μm emission are coincident with each other, proving that dust is present within HII regions. Both the radio continuum and 24 μm emission terminate close to the inner face of the 8 μm shell.

In HII regions dominated by stellar winds, typically those ionized by stars hotter than a spectral class O6, the immediate volume around the star is evacuated of both gas and dust producing a dip in 24 μm and radio continuum brightness, otherwise the 24 μm and radio continuum all peak at the location of the ionizing star(s). A detailed analysis of the infrared emission from the bubble N10 indicates the mid-infrared emission is due to stochastic heating, and subsequent cooling, of very small dust grains by the absorption of single UV photons (Watson et al. 2008). Everett and Churchwell (2010) have shown that the mass of dust in the N49 H2 region is very small, ~ 0.02 $M_\odot$, and absorbs <4% of the stellar UV photons within the hot wind-shocked region of the nebula.

The fact that dust appears to be well mixed within the hot, wind-shocked H$^+$ gas has several implications (Everett and Churchwell 2010). First, HII regions are somewhat older than their dynamical ages would imply, i.e., their radii are smaller at a given age than they would be in the absence of dust. Second, the lifetime of dust in the hostile environment around hot stars must either be $\geq 10^6$ years, the minimum age of several well-studied HII regions, or else the dust must be continuously replenished. One source of dust replenishment may be the slow photo-evaporation of small dense neutral globules that were overrun by the HII region I-front and/or the release of dust from debris disks around low-mass stars in the HII region as suggested by Koenig et al. (2008). Finally, because dust in these environments is highly positively charged, dust becomes the dominant coolant. For HII regions with X-ray emitting gas, dust cooling may lead to weaker X-ray emission and lower temperatures than would be the case in the absence of dust.

Although the observed mid-infrared "bubbles" have generally been interpreted as projected three-dimensional shells, c.f. Watson et al. (2008), CO observations of a sample of these objects provide a new puzzle (Beaumont and Williams 2010). These observations show a ring of CO coincident with the the mid-infrared rings, but no evidence of CO in the center of the bubble, suggesting that these objects are true rings or tori observed face on. Beaumont and Williams (2010) infer from this that the parent molecular clouds are more sheet-like, i.e., thin in one dimension and extended in two dimensions. If this is the case, ionized gas should have a bipolar distribution with extended emission perpendicular to the thin dimension of the molecular sheet. MAGPIS 20 cm images (Helfand et al. 2006) do not indicate bipolar morphologies, but this could be because extended emission has been filtered out by the VLA. Cazzolato and Pineault (2005) also showed that expanding shells typically do not show line emission toward

their centers, even if they are surrounded by an exterior shell, due to turbulent and thermal gas motions in the shell. Further multiwavelength observations of these bubbles will be needed to resolve the question of the true bubble morphology.

A final interesting point is the relationship of these bubbles to multiple generations, or "triggered" star formation. Numerous YSOs and small secondary bubbles (presumably produced by second-generation triggered star formation) are apparent on the periphery of larger primary bubbles (presumably produced by first-generation O and B stars). ❯ *Figure 9-15* shows an example of this phenomenon. YSOs were detected toward about 13% of the *Spitzer*/GLIMPSE sample of bubbles (Churchwell et al. 2007, 2006). Two mechanisms have been hypothesized for triggered star formation: (1) the Collect and Collapse (CC) model of Elmegreen and Lada (1977), and (2) the Radiation Driven Implosion (RDI) model of Bertoldi (1989). Deharveng and coworkers (see Deharveng et al. (2009) and references therein) have all identified YSOs toward numerous MIR bubbles. They find evidence for both CC and RDI formation mechanisms in compressed PDR envelopes around HII regions.

The coincidence of the PAH bubbles and these YSOs, in addition to the presence of secondary bubbles super-imposed on larger bubbles seem compelling evidence for triggered star formation. However, it is essentially impossible to prove that the YSOs would not have spontaneously formed in the absence of the HII region. Even if the YSOs on the peripheries of HII
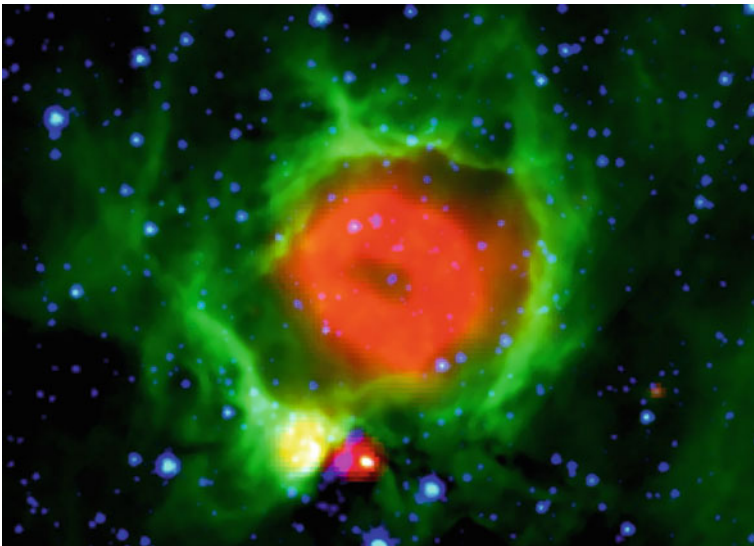
⬛ Fig. 9-15

An image of the MIR wind-dominated bubble N49 composed of GLIMPSE/MIPSGAL images from Churchwell et al. (2006) with 4.5 μm (*blue*), 8.0 μm (*green*), and 24 μm (*red*). An O5 V star is located in a dip at the center. A bright 24 μm shell of thermal dust emission surrounds the central dip which is within the hot wind-shocked, ionized gas. A PDR shell traced by 8 μm emission surrounds the H2 region. Along the bottom of the PDR shell there are three YSOs; the right most is bright at 24 μm, the middle one is an EGO with extended emission at 4.5 μm and is also bright at 24 μm, the left most with the yellow color is a compact H2 region and is bright at 24 and 8 μm. These suggest triggered star formation

regions were triggered by the HII region, only 10–15% of bubbles show probable evidence of triggering (Churchwell et al. 2006) suggesting that this mechanism, although important for astrophysical reasons, may not be the dominant star formation mechanism.

4.4 Massive Star Formation Regions: A Case Study

Massive star formation regions (MSFRs) are rare but important. They produce the bulk of the radiant energy in the Galaxy, are responsible for heavy element enrichment of the ISM, impact the dynamics of the ISM in their neighborhoods via stellar winds and radiation pressure, heat their natal molecular clouds, and drive complex exothermic chemical reactions. They are also very prominent at mid-infrared wavelengths. Due to their intense UV photon fluxes and strong stellar winds, MSFRs generally have a central wind-evacuated region surrounded by a shocked, very hot plasma outside of which is a photodissociated (PDR) shell. These are the stars responsible for producing the bubbles discussed in the previous section and for ultimately dispersing their natal molecular cloud.

For many years, our understanding of massive star formation regions relied on detailed investigation of the Orion nebula which is close enough that extinction (in the optical), or limited angular resolution, and sensitivity (in the infrared) were not insurmountable obstacles. With current instrumentation, detailed investigations of the stellar and interstellar content of hundreds of MSFRs are now possible. Here we summarize what has been learned for one nearby example, M17.

M17 is among the most massive and youngest star formation regions within 2 kpc of the Sun. Povich et al. (2007) present a recent analysis of the spectral energy distribution of M17 as a function of wavelength from ~1 μm to 90 cm. In particular, they identified changes in the SEDs corresponding to additional emission in the *Spitzer*/IRAC [3.6], [5.8], and [8.0] bands beyond what would be expected from thermal dust emission. This excess emission is produced by PAHs. This work also presented evidence that PAHs are destroyed in the M17 HII region by characterizing the spatial variation of the *Spitzer*/IRAC [4.5] band (which contains no PAH feature) to the other bands (❯ *Fig. 9-16*). The destruction of PAHs in the region of ionized gas was confirmed with *Spitzer*/IRS spectra taken at four locations (❯ *Fig. 9-17*). These spectra showed a rapid drop in PAH emission as one moves from the PDR region across the M17 SW arm into the HII region.

This study also showed the presence of hot, diffuse, soft X-ray emitting gas in the central cavity between the SW and N arms of M17 (❯ *Fig. 9-18*). The hot X-ray emitting gas appears to be flowing unopposed from the central cavity where the two arms of M17 open outward. This illustrates the expected general morphology of MSFRs (and wind-shocked HII regions) that contain multiple massive stars with strong winds, namely, a hot, wind-shocked X-ray emitting central cavity, surrounded by a shell of warm thermally emitting dust that is bright at 20–30 μm and lies inside the cooler $\sim 10^4$ K ionized hydrogen traced by radio continuum emission. The PDR traced by PAH emission (IRAC bands [5.8] and especially [8.0]) forms an envelope around both the north and southwest arms of M17.

The more recent study of Povich et al. (2009) puts M17 into an even larger context (❯ *Fig. 9-19*), finding a mid-infrared bubble, M17EB, with a diameter of $\sim 0.°5$ (17.5 pc at a distance of 2 kpc). This bubble is bounded on one side by the M17 HII region and the other side by the molecular cloud, MC G15.9-0.7. Star formation is also present where the M17EB bubble impinges on this molecular cloud. M17EB and MC G15.9-0.7 are seen in CO (2-1) emission
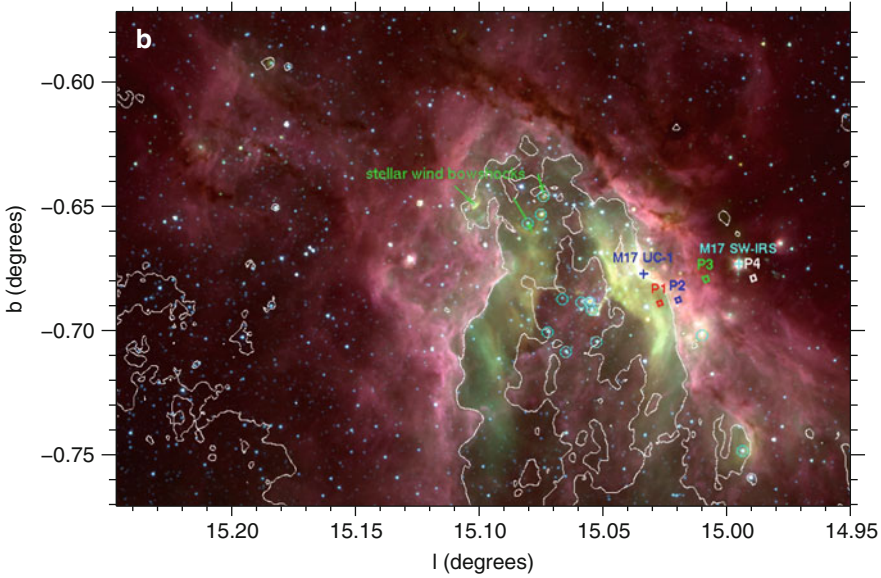
◘ Fig. 9-16

M17 in IRAC bands [3.6]-*blue*, [4.5]-*green*, and [5.8]-*red*. O stars are indiced by cyan circles, wind-blown bow shocks are indicated by green arrows, and the boxes labeled *P1-P4* show the locations of IRS spectra, using the same color coding as the spectra in the right figure. *P1* probes the H2 region; *P2&P3* probe the PDR region along the M17 SW arm, and *P4* probes the M17SW molecular cloud. The white contours show the region inside of which PAHs have been destroyed, as determined from the ratio of [5.8]/[4.5]. Figure from Povich et al. (2007)
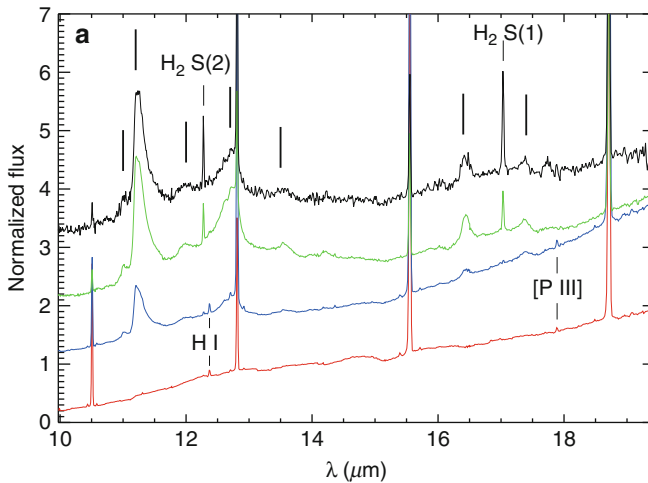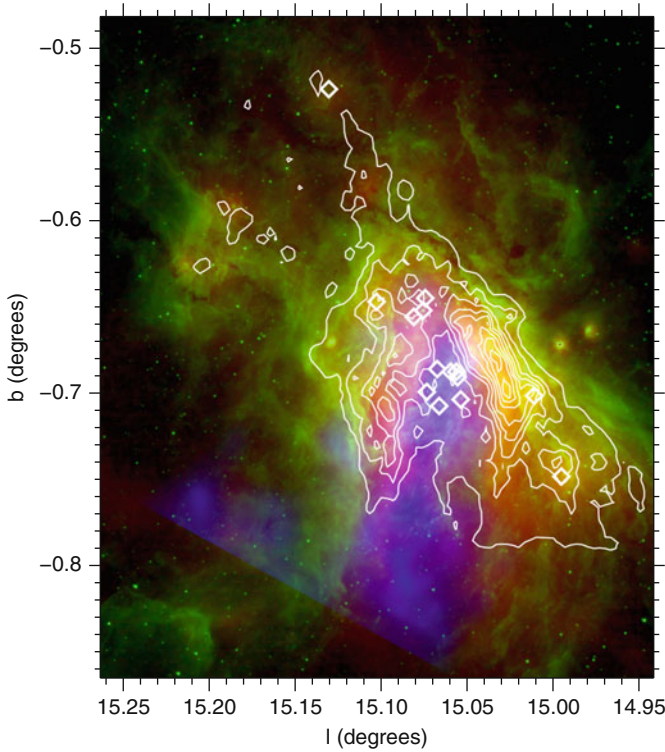

◘ Fig. 9-17

***Spitzer*/IRS spectra at locations *P1-P4* shown in ❯ *Fig. 9-16*. The spectra have been vertically shifted for clarity. Note the spectral change from nebular fine structure lines at *P1*, to increasing intensity of PAHs at *P2* and *P3*, to an increasing intensity of H2 lines from *P2* to *P4*. Figure from Povich et al. (2007)**
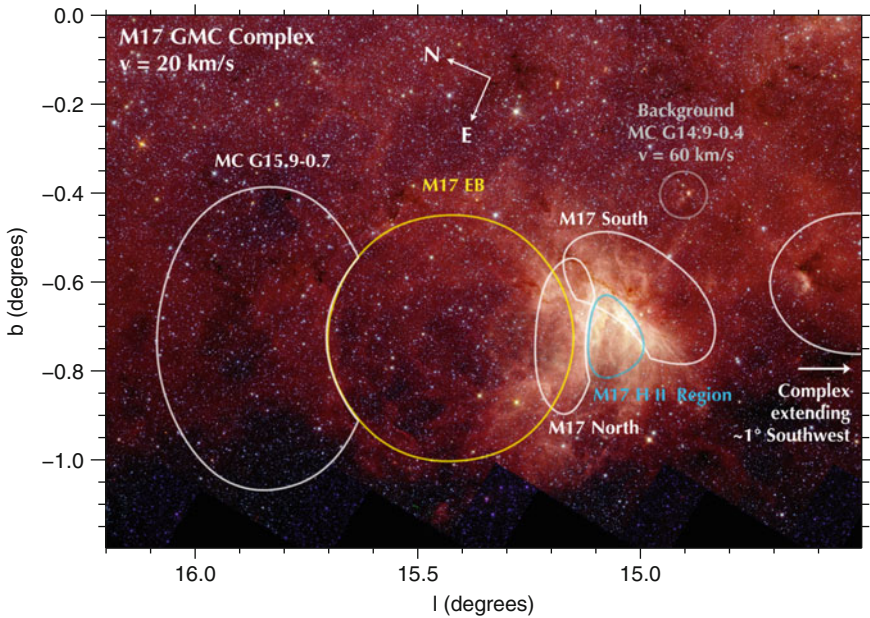
◼ Fig. 9-18

A composite color image of M17 showing soft X-ray diffuse emission (0.5–2.0 keV) in blue, thermal dust emission at 21.3 μm MSX emission in red, and PAH emission from IRAC [5.8] in green. The white contours show 20 cm continuum emission indicating the distribution of ~ 10^4 K ionized gas. Image from Povich et al. (2007)

(❯ *Fig. 9-20*) at the same velocity as M17 (~19 km s^{-1}). The CO data indicate a gas mass of ~1.4×10^5 $M_\odot$ in the velocity range 12–26 km s^{-1}.

YSO candidates were identified throughout the entire M17 complex using both MIR color-color analyses and the spectral energy distribution (SED) analyses using the Monte Carlo radiative transfer models of massive YSOs developed by Whitney et al. (2004) combined with the model-fitting routine of Robitaille et al. (2007b). A control field was used to estimate the fraction of contamination by unassociated YSOs, which in this part of the Galactic plane is about 50%! Five candidate ionizing stars of M17EB were identified near the center of M17EB with an estimated age of 2–5 Myr, compared to ~0.5 Myr for stars with mass ≥ 3$M_\odot$ in the ionizing cluster of M17 (NGC6618). The YSO populations are concentrated in M17 itself, along the periphery of M17EB, near the center of M17EB, and in MC G15.9-0.7. Based on relative ages and locations, it seems plausible that NGC6618, the ionizing cluster of M17, may have been triggered by the older cluster responsible for the creation and ionization of M17EB. The expansion of M17EB may also be triggering current star formation in MC G15.9-0.7. It was also

◧ Fig. 9-19
A schematic diagram showing the approximate locations and boundaries of several large-scale features associated with the M17 H2 region superimposed on a GLIMPSE [5.8]-*red*, [4.5]-*green*, and [3.6]-*blue* image (Povich et al. **2009**). Labeled features are discussed in the text

noted that essentially all the O stars in NGC6618 are likely to be binary systems for consistency with the inferred UV photon flux and current distance estimates to M17.

5   Evolved Stars

In the course of their evolution nearly all stars will lose mass, some of which will condense into dust. Infrared observations are thus important for determining the effect of this mass loss on stellar evolution and constraining the return of processed material to the interstellar medium. We review some of the results working our way upward in mass, but starting with a brief summary of stellar variability in the infrared.

5.1   Variable Stars

At some level all stars are variable, but stars with periodic variability or massive stars with significant mass loss have been important in the history of astronomy. Cepheid variables are among the key standard candles in setting the extragalactic distance scale. RR Lyrae stars were used for one of the first determinations of the distance to the center of the Galaxy. Evolved massive stars are frequently large amplitude and long period variables; study of these sources are key
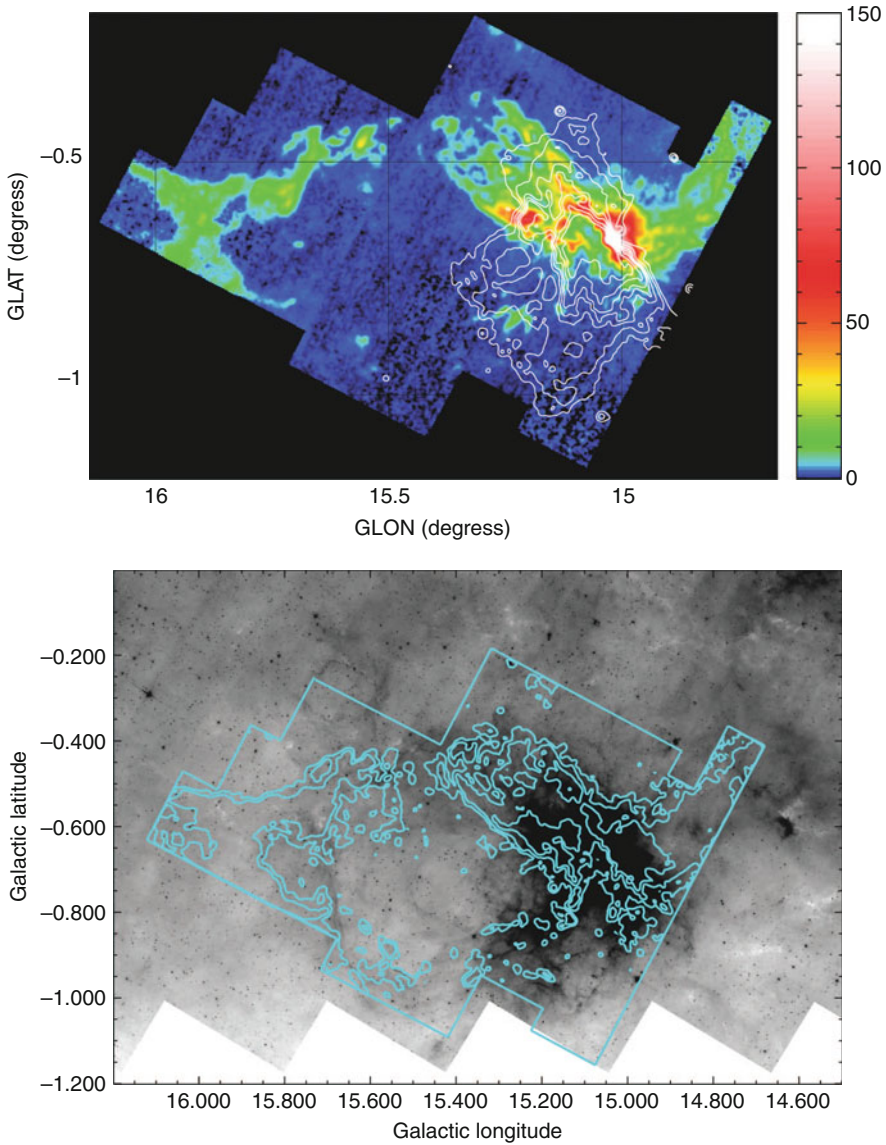
■ **Fig. 9-20**

[*Top*]. A ^{13}CO$(1-0)$ image of M17 and part of the M17EB shell (color with $T_A \Delta v (12-26$ km s$^{-1})$ in K km s^{-1} shown in the scale bar at right) obtained with the Heinrich Hertz Telescope (HHT). The contours are 90 cm VLA observations at intervals of 5, 10, 20, 30, 40, 60, and 80% of peak, which traces H$^+$ emission. [*Bottom*] The HHT ^{12}CO$(1-0)$ emission at 19 km s^{-1} superimposed on the GLIMPSE [8.0] image. The large M17EB molecular shell is clearly apparent in CO as well as at 8 μm emission. Figure from Povich et al. (**2009**)

for understanding the role of mass loss in stellar evolution as well as constraining the return of chemically enriched material into the interstellar medium. The variability associated with mass transfer and eclipses in binary systems provides important constraints on models of stellar evolution. Several programs are dedicated to searching for microlensing, but have also turned up large numbers of other variable sources in abundance.
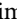
With the exception of the work on evolved stars, most of the study of variable stars has been the domain of optical astronomy. Large-scale deep surveys, e.g., the Optical Gravitational Lensing Experiment (OGLE), have produced a catalog of 200,000 potentially variable sources (Wozniak et al. 2002) in selected low-extinction directions, like Baades window. But it is often noted that the two principal difficulties using optical surveys of variable stars to probe the structure of the Galaxy have been extinction and lack of uniform coverage (Paczynski 1997).

Surprisingly, only the ongoing near-infrared VVV survey (Minniti et al. 2010) has been designed to produce the light curves needed to identify different classes of variable sources. Most previous surveys, with only a few epochs of observation, only allow for variable sources to be flagged. These studies tend to preferentially select large-amplitude or long-period variables. For example, Robitaille et al. (2007a) used the MSX and GLIMPSE/MIPSGAL surveys to identify candidate mid-infrared variables by comparing flux densities at 8.0 vs 8.28 μm and secondarily at 24 vs 21.3 μm. By requiring that the amplitude of variation exceed a factor of two, the number of candidate-variable sources was winnowed from almost 52,000 sources to 592, most of which are expected to be asymptotic giant branch stars.

5.2 Asymptotic Giant Stars

During the asymptotic giant branch (AGB) phase of low and intermediate mass stars, stars develop dusty circumstellar shells. These stars provide a significant source of carbon and oxygen and dust to the interstellar medium; an extensive review can be found in Habing (1996). A survey of the LMC (Srinivasan et al. 2009), which has the advantage that the sources are at a common distance and extinction, used infrared SEDs to identify different classes of AGB stars, finding that the dust mass returned to the LMC from these sources is 6-13 $\times$ 10^{-3} $M_\odot$ yr^{-1}. Using a catalog of red GLIMPSE objects, Robitaille et al. (2008) compared the observed Galactic distribution to a synthetic distribution, assuming that Galactic AGB stars have similar infrared colors to those in the LMC. They estimate that 30–50% of the 22,000 red sources are AGB stars. Much more work characterizing the galactic population of AGB stars remains to be done.

5.3 Planetary Nebulae

The mid-infrared colors of planetary nebulae strongly overlap with HII regions and young stellar objects (YSOs). The identification of PN in the mid-infrared therefore requires confirming images or spectra. In ❯ *Fig. 9-21*, a montage of PNe images from the GLIMPSE survey are shown to illustrate some of the morphologies seen in the IRAC bands. Kwok et al. (2008) analyzed the SEDs for 30 previously identified PNe in the GLIMPSE survey. Phillips and Ramos-Larios (2008b) used 2MASS and GLIMPSE, finding that although their colors are very similar to HII regions for identification purposes, their intensity profiles have broad wings that increase with wavelength which they attribute to a photodissociation region (PDR) around PNe. Using this, they identified a set of candidate PNe (Phillips and Ramos-Larios 2008a) that await
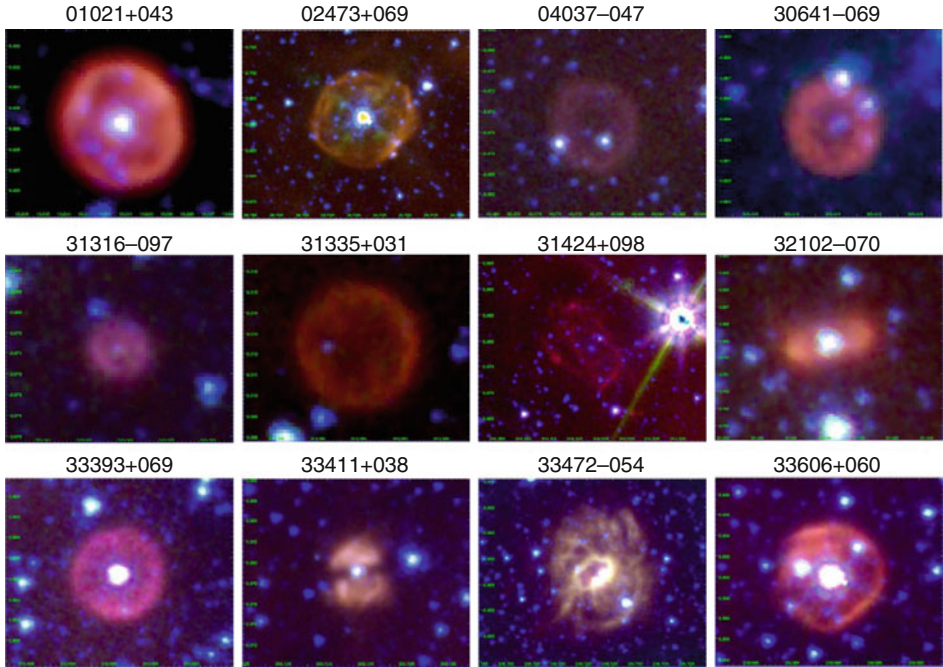
◧ Fig. 9-21

A montage of several planetary nebulae seen in the GLIMPSE survey. Colors are [8.0]-*red*, [4.5]-*green*, and [3.6]-*blue*

spectroscopic confirmation. Hora et al. (2006, 2004) report *Spitzer*/IRAC observations of several PNe, including the Helix nebula. They found these objects are quite red, $[3.6] - [4.5] > 0.6$ and $[5.8] - [8.0] > 1.0$, whereas the central stars are ~0 in both colors. They also suggest that the [8.0] band may have significant contributions from H_2 and [ArIII] line emission.

PNe have also been imaged with *Spitzer*/MIPS. Observations of NGC2346 (Su et al. 2004) show an edge-on toroid at 70 μm, the tips of the bipolar outflow at 24 μm, and indicate that dust resides in the ionized nebula. The Helix nebula (Su et al. 2007) shows a debris disk of dust mass ~ $0.13 M_\odot$ around the central star based on the observed SED. The 24 μm images also show very bright emission surrounding the central star, indicating dust close to the star. This they interpret as further evidence for a debris disk. Their IRS spectrum also shows a bright [OIV] 25.9 μm emission line contribution to the 24 μm band. NGC 650 also appears to have a nearly edge-on torus (Ueta 2006) as well as 24 μm emission around the central star. As more far-infrared data become available, more new insights on the nature of PNe are expected.

5.4 Luminous Blue Variables and Wolf-Rayet Stars

One of the surprises of the MIPSGAL survey was the presence of (at least) 416 disk and ring sources seen in 24 μm (Mizuno et al. 2010), which break into 54 objects with central sources, 112 rings, 226 disks, 24 two-lobed objects, two filamentary, and 10 miscellaneous objects.

Approximately 80% of these objects have no 8 μm counterpart indicating that most of them are probably not PAH bubbles or standard HII regions. Further work (Gvaramadze et al. 2010; Mizuno et al. 2010; Wachter et al. 2010) has shown that these sources are a heterogenous set, including some planetary nebulae and circumstellar envelopes around giant and supergiant stars.

However, a significant fraction of these sources are associated with various stages of massive star evolution. Near- and mid-infrared studies, c.f. Mauerhan et al. (2009) and references therein, have increased the sample of known Wolf-Rayet stars by 30%. When surveys and spectroscopic follow-up are complete, the sample is likely to more than double. Some of the sources associated with the 24 μm shells have been found to be Be stars and Wolf-Rayet stars. Most significantly, several shells are associated with Luminous Blue Variables (LBVs). These stars are thought to be a short-lived stage of massive star evolution, preceding the Wolf-Rayet phase, during which the star loses a significant fraction of its mass. Studies of these phases of massive star evolution have always been dogged by small sample sizes. With these new infrared-selected candidates, that may soon change.
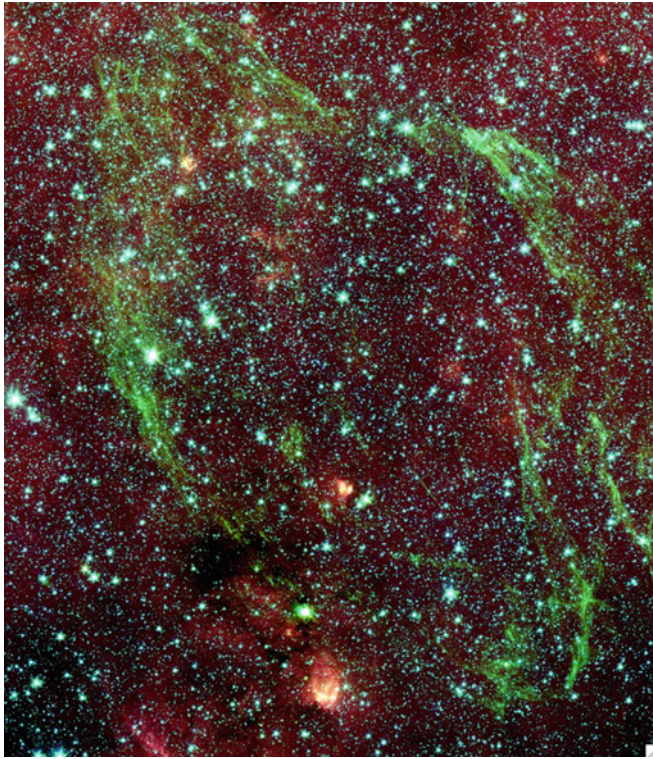
5.5 Supernova Remnants

Supernova remnants (SNRs) generally do not stand out in the mid-infrared, unless they occur in the vicinity of molecular gas. Reach et al. (2006) visually searched the GLIMPSE images for all 95 known SNRs that lie in the survey area. Only 18 (19%) of the SNRs were unambiguously detected. The low detection rate may have several causes: confusion with HII regions, shock velocities that do not produce emission lines in the *Spitzer*/IRAC bands, and the contamination of mid-infrared diffuse emission with SNR shell emission. Some, but not all, of the 18 SNRs are traced by excess emission in the [4.5] band due to lines of shocked molecular hydrogen. This includes W44 (❯ *Fig. 9-22*), G311.5-0.3, and RCW103. This work also shows how SNRs can produce a wide range of mid-infrared molecular and atomic line emission. The variation in these emission lines from object to object, and even within a single object, mean that SNRs cannot be isolated to a small color-color space at mid-infrared wavelengths.

6 Limitations and Lessons Learned

Before the opening of the infrared frontier, the study of stars, star formation, and interstellar medium was the domain of the optical and radio astronomers. Looking back on what infrared investigations have revealed so far, it is instructive to reflect on where these previous eras were limited, and where new opportunities may lie.

The unbreachable limitation on optical investigations of the Galaxy is the patchy extinction principally, but not exclusively, found along the plane of the Galaxy. As a result, most of the inner Milky Way will forever be off-limits to the optical astronomer. This limitation affects much of the triaxial bulge and also means that all of the Galactic disk more distant than a few kiloparsecs is unreachable. As new optical surveys come on line to probe the time-variation, parallax, proper motions, radial velocities, and metallicities of stellar sources, it will be important to remember this limitation.

■ Fig. 9-22

GLIMPSE image of W44, one of the few supernova remnants to show clear mid-infrared emission, due to emission from shocked molecular hydrogen. See Reach et al. (2006) for more details

In contrast, radio surveys of the Galaxy, which suffer no extinction, have been limited principally by angular resolution. Until very recently with VLA 6 cm CORNISH Galactic Plane Survey (Purcell et al. 2008), there have been no radio surveys of the Galactic plane that come close to matching the ~ arcsec resolution available to optical and infrared surveys. This limitation also produces a distance bias in Galactic investigations, since distant clouds and star formation regions are unresolved. As a result, most of the focus has been on the more nearby resolved structures.

The combination of these two selection effects, extinction at optical wavelengths and angular size for radio wavelength surveys, means that beyond a few kiloparsecs from the Sun our knowledge of the Galaxy is grossly incomplete. In his introduction to the two-volume, 1,900-page handbook of star formation regions in the Galaxy, Reipurth (2008) notes that all of the star formation regions described in the volumes lie within ~2 kpc of the Sun. Students looking to get into Galactic astronomy should take heart. Most of the Galaxy yet remains to be explored!

Although infrared studies of the Galaxy have the advantage of low extinction and high angular resolution (and sensitivity), they too have limitations that must be borne in mind. The flip side of low extinction and a large number of sources is source confusion. Confusion imposes a brightness limitation on stellar catalogues that will vary with direction. Moreover, the current

generation of infrared surveys are all photometric. Very few velocity-resolved infrared *spectral* surveys, either for the stellar component or the diffuse emission, are on the horizon. This means that velocities, and therefore kinematic distances, require follow-up at other wavelengths.

Finally, a limitation that has dogged all Galactic investigations is the issue of sky coverage. In order to draw conclusions about the structure of the whole Galaxy it is wise to survey the entire Galaxy (or at the very least the full Galactic plane). This is particularly challenging for ground-based studies as it requires two observing sites. In this respect, infrared Galactic astronomy has been fortunate as it has come of age at the same time that data acquisition and analysis software are up to the task. But synthesis of all of this data into useful knowledge will remain a challenge for us all. Galactic astronomy has a lot of trees to distract us. But we are definitely making progress on understanding the forest.

Acknowledgments

Cross-References

References

Abergel, A., Bernard, J. P., Boulanger, F., Cesarsky, C., Desert, F. X., Falgarone, E., Lagache, G., Perault, M., Puget, J.-L., Reach, W. T., Nordh, L., Olofsson, G., Huldtgren, M., Kaas, A. A., Andre, P., Bontemps, S., Burgdorf, M., Copet, E., Davies, J., Montmerle, T., Persi, P., & Sibille, F. 1996, A&A, 315, L329

Abergel, A., Bernard, J. P., Boulanger, F., Desert, F. X., Lagache, G., Puget, J. L., Reach, W. T., Falgarone, E., Nordh, L., Olofsson, G., Andre, P., Bacmann, A., & Ristorcelli, I. 1998, Star Formation with the Infrared Space Observatory, 132, 220

Alard, C. 2001, A&A, 379, L44

Alexander, M. J., Kobulnicky, H. A., Clemens, D. P., Jameson, K., Pinnick, A., & Pavel, M. 2009, AJ, 137, 4824

Alves, D. R. 2000, ApJ, 539, 732

Andre, P., Ward-Thompson, D., & Barsony, M. 2000, Protostars and Planets IV, eds. V. Mannings, A. P. Boss, S. S. Russell (Tucson: University of Arizona Press), 59

Andre, P., Ward-Thompson, D., & Motte, F. 1996, A&A, 314, 625

Athanassoula, E. 2007, MNRAS, 377, 1569

Babusiaux, C., Gomez, A., Hill, V., Royer, F., Zoccali, M., Arenou, F., Fux, R., Lecureur, A., Schultheis, M., Barbuy, B., Minniti, D., & Ortolani, S. 2010, A&A, 519, 77

Bacmann, A., Andre, P., Abergel, A., Bernard, J. P., Puget, J. L., Bontemps, S., & Ward-Thompson, D. 1998, Star Formation with the Infrared Space Observatory, 132, 307

Bakos, J., Trujillo, I., & Pohlen, M. 2008, ApJ, 683, L103

Bania, T. M., Anderson, L. D., Balser, D. S., & Rood, R. T. 2010, ApJL, 718, L106

Beaumont, C. N., & Williams, J. P. 2010, ApJ, 709, 791

Beichman, C. A., Neugebauer, G., Habing, H. J., Clegg, P. E., & Chester, T. J. 1988, Infrared astronomical satellite (IRAS) catalogs and atlases, 1, 1

Benjamin, R. A., Churchwell, E., Babler, B. L., Bania, T. M., Clemens, D. P., Cohen, M., Dickey, J. M., Indebetouw, R., Jackson, J. M., Kobulnicky, H. A., Lazarian, A., Marston, A. P., Mathis, J. S., Meade, M. R., Seager, S., Stolovy, S. R., Watson, C., Whitney, B. A., Wolff, M. J., & Wolfire, M. G. 2003, PASP, 115, 953

Benjamin, R. A., Churchwell, E., Babler, B. L., Indebetouw, R., Meade, M. R., Whitney, B. A., Watson, C., Wolfire, M. G., Wolff, M. J., Ignace, R., Bania, T. M., Bracker, S., Clemens, D. P., Chomiuk, L., Cohen, M., Dickey, J. M., Jackson, J. M., Kobulnicky, H. A., Mercer, E. P., Mathis, J. S., Stolovy, S. R., & Uzpen, B. 2005, ApJ, 630, L149

Bergin, E. A., & Tafalla, M. 2007, ARAA, 45, 339

Bertoldi, F. 1989, ApJ, 346, 735

Binney, J., Gerhard, O. E., Stark, A. A., Bally, J., & Uchida, K. I. 1991, MNRAS, 252, 210

Binney, J., & Merrifield, M. 1998, Galactic Astronomy (Princeton: Princeton University Press)

Binney, J., & Tremaine, S. 2008, Galactic Dynamics (2nd ed.; Princeton: Princeton University Press)

Bissantz, N., Englmaier, P., & Gerhard, O. 2003, MNRAS, 340, 949

Blitz, L., & Spergel, D. N. 1991, ApJ, 379, 631

Block, D. L., Buta, R., Knapen, J. H., Elmegreen, D. M., Elmegreen, B. G., & Puerari, I. 2004, AJ, 128, 183

Block, D. L., & Wainscoat, R. J. 1991, Nature, 353, 48

Boggess, N. W., Mather, J. C., Weiss, R., Bennett, C. L., Cheng, E. S., Dwek, E., Gulkis, S., Hauser, M. G., Janssen, M. A., Kelsall, T., Meyer, S. S., Moseley, S. H., Murdock, T. L., Shafer, R. A., Silverberg, R. F., Smoot, G. F., Wilkinson, D. T., & Wright, E. L. 1992, ApJ, 397, 420

Brown, J. C., Haverkorn, M., Gaensler, B. M., Taylor, A. R., Bizunok, N. S., McClure-Griffiths, N. M., Dickey, J. M., & Green, A. J. 2007, ApJ, 663, 258

Burton, W. B., Deul, E. R., & Liszt, H. S. 1992, in Saas-Fee Advanced Course of the Swiss Society for Astrophysics and Astronomy: The Galactic Interstellar Medium, (New York: Springer-Verlag), 1

Burton, W. B., Gordan, M. A., Bania, T. M., & Lockman, F. J. 1975, ApJ, 202, 30

Buta, R., & Combes, F. 1996, Fundamentals of Cosmic Physics, 17, 95

Carey, S. J., Noriega-Crespo, A., Mizuno, D. R., Shenoy, S., Paladini, R., Kraemer, K. E., Price, S. D., Flagey, N., Ryan, E., Ingalls, J. G., Kuchar, T. A., Gonçalves, D. P., Indebetouw, R., Billot, N., Marleau, F. R., Padgett, D. L., Rebull, L. M., Bressert, E., Ali, B., Molinari, S., Martin, P. G., Berriman, G. B., Boulanger, F., Latter, W. B., Miville-Deschenes, M. A., Shipman, R., & Testi, L. 2009, PASP, 121, 76

Cazzolato, F., & Pineault, S. 2005, AJ, 129, 2731

Churchwell, E. 2002, ARAA, 40, 27

Churchwell, E., Babler, B. L., Meade, M. R., Whitney, B. A., Benjamin, R., Indebetouw, R., Cyganowski, C., Robitaille, T. P., Povich, M., Watson, C., & Bracker, S. 2009, PASP, 121, 213

Churchwell, E., Povich, M. S., Allen, D., Taylor, M. G., Meade, M. R., Babler, B. L., Indebetouw, R., Watson, C., Whitney, B. A., Wolfire, M. G., Bania, T. M., Benjamin, R. A., Clemens, D. P., Cohen, M., Cyganowski, C. J., Jackson, J. M., Kobulnicky, H. A., Mathis, J. S., Mercer, E. P., Stolovy, S. R., Uzpen, B., Watson, D. F., & Wolff, M. J. 2006, ApJ, 649, 759

Churchwell, E., Watson, D. F., Povich, M. S., Taylor, M. G., Babler, B. L., Meade, M. R., Benjamin, R. A., Indebetouw, R., & Whitney, B. A. 2007, ApJ, 670, 428

Clark, J. S., Negueruela, I., Davies, B., Larionov, V. M., Ritchie, B. W., Figer, D. F., Messineo, M., Crowther, P. A., & Arkharov, A. A. 2009, A&A, 498, 109

Cohen, M., Walker, R. G., Jayaraman, S., Barker, E., & Price, S. D. 2002, AJ, 121, 1180

Cole, A. A., & Weinberg, M. D. 2002, ApJ, 574, L43

Cragg, D. M., Johns, K. P., Godfrey, P. D., & Brown, R. D. 1992, MNRAS, 259, 203

Cragg, D. M., Sobolev, A. M., & Godfrey, P. D. 2005, MNRAS, 360, 533

Cyganowski, C. J., Brogan, C. L., Hunter, T. R., & Churchwell, E. 2009, ApJ, 702, 1615

Cyganowski, C. J., Whitney, B. A., Holden, E., Braden, E., Brogan, C. L., Churchwell, E., Indebetouw, R., Watson, D. F., Babler, B. L., Benjamin, R., Gomez, M., Meade, M. R., Povich, M. S., Robitaille, T. P., & Watson, C. 2008, AJ, 136, 2391

Dame, T. M., Hartmann, D., & Thaddeus, P. 2001, ApJ, 547, 792

Dame, T. M., & Thaddeus, P. 2008, ApJ, 683, L143

De Buizer, J. M. D., & Vacca, W. D. 2010, AJ, 140, 196

Debattista, V. P., & Shen, J. 2007, ApJ, 654, L127

Deharveng, L., Zavagno, A., Schuller, F., Caplan, J., Pomarès, M., & Breuck, C. D. 2009, A&A, 496, 177

Devine, K. 2009, PhD Thesis, U of Wisconsin-Madison

Diehl, R., Halloin, H., Kretschmer, K., Lichti, G. G., Schönfelder, V., Strong, A. W., von Kienlin, A., Wang, W., Jean, P., Knödlseder, J., Roques, J.-P., Weidenspointner, G., Schanne, S., Hartmann, D. H., Winkler, C., & Wunderer, C. 2006, Nature, 439, 45

Draine, B. T. 2003, ARAA, 41, 241

Draine, B. T., Dale, D. A., Bendo, G., Gordon, K. D., Smith, J. D. T., Armus, L., Engelbracht, C. W., Helou, G., Kennicutt, R. C., Li, A., Roussel, H., Walter, F., Calzetti, D., Moustakas, J., Murphy, E. J., Rieke, G. H., Bot, C., Hollenbach, D. J., Sheth, K., & Teplitz, H. I. 2007, ApJ, 663, 866

Draine, B. T., & Li, A. 2001, ApJ, 551, 807

Drimmel, R. 2000, A&A, 358, L13

Drimmel, R., Cabrera-Lavers, A., & López-Corredoira, M. 2003, A&A, 409, 205

Drimmel, R., & Spergel, D. N. 2001, ApJ, 556, 181

Durant, M., & van Kerkwijk, M. H. 2006, ApJ, 650, 1070

Dwek, E., Arendt, R. G., Hauser, M. G., Kelsall, T., Lisse, C. M., Moseley, S. H., Silverberg, R. F., Sodroski, T. J., & Weiland, J. L. 1995, ApJ, 445, 716

Elmegreen, B. G., & Lada, C. J. 1977, ApJ, 214, 725

Englmaier, P., & Gerhard, O. 1999, MNRAS, 304, 512

Erwin, P., Pohlen, M., & Beckman, J. E. 2008, AJ, 135, 20

Everett, J. E., & Churchwell, E. 2010, ApJ, 713, 592

Fich, M., Blitz, L., & Stark, A. A. 1989, ApJ, 342, 272

Fouqué, P., Chevallier, L., Cohen, M., Galliano, E., Loup, C., Alard, C., de Batz, B., Bertin, E., Borsenberger, J., Cioni, M. R., Copet, E., Dennefeld, M., Derriere, S., Deul, E., Duc, P.-A., Egret, D., Epchtein, N., Forveille, T., Garzón, F., Habing, H. J., Hron, J., Kimeswenger, S., Lacombe, F., Bertre, T. L., Mamon, G. A., Omont, A., Paturel, G., Pau, S., Persi, P., Robin, A. C., Rouan, D., Schultheis, M., Simon, G., Tiphène, D., Vauglin, I., & Wagner, S. J. 2000, A&A Supp, 141, 313

Freeman, K. C. 1970, ApJ, 160, 811

Freudenreich, H. T. 1998, ApJ, 492, 495

Freudenreich, H. T., Berriman, G. B., Dwek, E., Hauser, M. G., Kelsall, T., Moseley, S. H., Silverberg, R. F., Sodroski, T. J., Toller, G. N., & Weiland, J. L. 1994, ApJ, 429, L69

Fux, R. 1999, A&A, 345, 787

Gao, J., Jiang, B. W., & Li, A. 2009, ApJ, 707, 89

Georgelin, Y. M., & Georgelin, Y. P. 1976, A&A, 49, 57

Gerhard, O. 2002, in The Dynamics, Structure & History of Galaxies: A Workshop in Honour of Professor Ken Freeman, eds. G.S. Da Costa & H. Jerjen, 273, 73

Ghez, A. M., Salim, S., Weinberg, N. N., Lu, J. R., Do, T., Dunn, J. K., Matthews, K., Morris, M. R., Yelda, S., Becklin, E. E., Kremenek, T., Milosavljevic, M., & Naiman, J. 2008, ApJ, 689, 1044

Gillessen, S., Eisenhauer, F., Fritz, T. K., Bartko, H., Dodds-Eden, K., Pfuhl, O., Ott, T., & Genzel, R. 2009, ApJL, 707, L114

Girardi, L., Groenewegen, M. A. T., Hatziminaoglou, E., & da Costa, L. 2005, A&A, 436, 895

Girardi, L., & Salaris, M. 2001, MNRAS, 323, 109

Green, J. A., McClure-Griffiths, N. M., Caswell, J. L., Ellingsen, S. P., Fuller, G. A., Quinn, L., & Voronkov, M. A. 2009, ApJL, 696, L156

Grocholski, A. J., & Sarajedini, A. 2002, AJ, 123, 1603

Groenewegen, M. A. T. 2008, A&A, 488, 935

Groenewegen, M. A. T., & Blommaert, J. A. D. L. 2005, A&A, 443, 143

Gvaramadze, V. V., Kniazev, A. Y., & Fabrika, S. 2010, MNRAS, 405, 1047

Habing, H. J. 1996, Astronomy and Astrophysics Review, 7, 97

Hammersley, P. L., Garzón, F., Mahoney, T. J., López-Corredoira, M., & Torres, M. A. P. 2000, MNRAS, 317, L45

Haslam, C. G. T., Salter, C. J., Stoffel, H., & Wilson, W. E. 1982, Astronomy and Astrophysics Supplement Series, 47, 1

Heitsch, F., Whitney, B. A., Indebetouw, R., Meade, M. R., Babler, B. L., & Churchwell, E. 2007, ApJ, 656, 227

Helfand, D. J., Becker, R. H., White, R. L., Fallon, A., & Tuttle, S. 2006, AJ, 131, 2525

Hora, J. L., Latter, W. B., Allen, L. E., Marengo, M., Deutsch, L. K., & Pipher, J. L. 2004, ApJSupp, 154, 296

Hora, J. L., Latter, W. B., Smith, H. A., & Marengo, M. 2006, ApJ, 652, 426

Indebetouw, R., Mathis, J. S., Babler, B. L., Meade, M. R., Watson, C., Whitney, B. A., Wolff, M. J., Wolfire, M. G., Cohen, M., Bania, T. M., Benjamin, R. A., Clemens, D. P., Dickey, J. M., Jackson, J. M., Kobulnicky, H. A., Marston, A. P., Mercer, E. P., Stauffer, J. R., Stolovy, S. R., & Churchwell, E. 2005, ApJ, 619, 931

Ishihara, D., Onaka, T., Kataza, H., Salama, A., Alfageme, C., Cassatella, A., Cox, N., García-Lario, P., Stephenson, C., Cohen, M., Fujishiro, N., Fujiwara, H., Hasegawa, S., Ita, Y., Kim, W., Matsuhara, H., Murakami, H., Müller, T. G., Nakagawa, T., Ohyama, Y., Oyabu, S., Pyo, J., Sakon, I., Shibai, H., Takita, S., Tanabé, T., Uemizu, K., Ueno, M., Usui, F., Wada, T., Watarai, H., Yamamura, I., & Yamauchi, C. 2010, A&A, 514, 1

Jackson, J. M., Finn, S. C., Rathborne, J. M., Chambers, E. T., & Simon, R. 2008, ApJ, 680, 349

Jackson, J. M., Rathborne, J. M., Shah, R. Y., Simon, R., Bania, T. M., Clemens, D. P., Chambers, E. T., Johnson, A. M., Dormody, M., Lavoie, R., & Heyer, M. H. 2006, ApJSupp, 163, 145

Jiang, B. W., Gao, J., Omont, A., Schuller, F., & Simon, G. 2006, A&A, 446, 551

Jiang, B. W., Omont, A., Ganesh, S., Simon, G., & Schuller, F. 2003, A&A, 400, 903

Johnston, K. J., Gaume, R., Stolovy, S., Wilson, T. L., Walmsley, C. M., & Menten, K. M. 1992, ApJ, 385, 232

Jurić, M., Ivezić, Ž., Brooks, A., Lupton, R. H., Schlegel, D., Finkbeiner, D., Padmanabhan, N., Bond, N., Sesar, B., Rockosi, C. M., Knapp, G. R., Gunn, J. E., Sumi, T., Schneider, D. P., Barentine, J. C., Brewington, H. J., Brinkmann, J., Fukugita, M., Harvanek, M., Kleinman, S. J., Krzesinski, J., Long, D., Neilsen, E. H., Nitta, A., Snedden, S. A., & York, D. G. 2008, ApJ, 673, 864

Kent, S. M., Dame, T. M., & Fazio, G. 1991, ApJ, 378, 131

Kerr, F. J., & Lynden-Bell, D. 1986, MNRAS, 221, 1023

Kessler, M. F., Steinz, J. A., Anderegg, M. E., Clavel, J., Drechsel, G., Estaria, P., Faelker, J., Riedinger, J. R., Robson, A., Taylor, B. G., & de Ferrán, S. X. 1996, A&A, 315, L27

Koenig, X. P., Allen, L. E., Gutermuth, R. A., Hora, J. L., Brunt, C. M., & Muzerolle, J. 2008, ApJ, 688, 1142

Kormendy, J., & Kennicutt, R. C. 2004, ARAA, 42, 603

Kurtz, S., Hofner, P., & Álvarez, C. V. 2004, ApJSupp, 155, 149

Kwok, S. 2007, Physics and Chemistry of the Interstellar Medium (Sausalito, CA: University Science Books)

Kwok, S., Zhang, Y., Koning, N., Huang, H.-H., & Churchwell, E. 2008, ApJSupp, 174, 426

Launhardt, R., Zylka, R., & Mezger, P. G. 2002, A&A, 384, 112

Liszt, H. S. 1985, in The Milky Way Galaxy: Proceedings of the 106th Symposium (Dordrecht: D. Reidel Publishing Co.), 283

Lockman, F. J. 1980, ApJ, 241, 200

López-Corredoira, M., Cabrera-Lavers, A., Garzón, F., & Hammersley, P. L. 2002, A&A, 394, 883

López-Corredoira, M., Cabrera-Lavers, A., Mahoney, T. J., Hammersley, P. L., Garzón, F., & González-Fernández, C. 2007, AJ, 133, 154

López-Corredoira, M., Hammersley, P. L., Garzón, F., Cabrera-Lavers, A., Castro-Rodríguez, N., Schultheis, M., & Mahoney, T. J. 2001, A&A, 373, 139

Lucas, P. W., Hoare, M. G., Longmore, A., Schröder, A. C., Davis, C. J., Adamson, A., Bandyopadhyay, R. M., de Grijs, R., Smith, M., Gosling, A., Mitchison, S., Gáspár, A., Coe, M., Tamura, M., Parker, Q., Irwin, M., Hambly, N., Bryant, J., Collins, R. S., Cross, N., Evans, D. W., Gonzalez-Solares, E., Hodgkin, S., Lewis, J., Read, M., Riello, M., Sutorius, E. T. W., Lawrence, A., Drew, J. E., Dye, S., & Thompson, M. A. 2008, MNRAS, 391, 136

Lutz, D., Feuchtgruber, H., Genzel, R., Kunze, D., Rigopoulou, D., Spoon, H. W. W., Wright, C. M., Egami, E., Katterloher, R., Sturm, E., Wieprecht, E., Sternberg, A., Moorwood, A. F. M., & de Graauw, T. 1996, A&A, 315, L269

Marshall, D. J., Fux, R., Robin, A. C., & Reylé, C. 2008, A&A, 477, L21

Marshall, D. J., Joncas, G., & Jones, A. P. 2009, ApJ, 706, 727

Marshall, D. J., Robin, A. C., Reylé, C., Schultheis, M., & Picaud, S. 2006, A&A, 453, 635

Martos, M., Hernandez, X., Yáñez, M., Moreno, E., & Pichardo, B. 2004, MNRAS, 350, L47

Mauerhan, J. C., van Dyk, S. D., & Morris, P. W. 2009, PASP, 121, 591

McClure-Griffiths, N. M., & Dickey, J. M. 2007, ApJ, 671, 427

McClure-Griffiths, N. M., Dickey, J. M., Gaensler, B. M., & Green, A. J. 2004, ApJ, 607, L127

Mellinger, A. 2009, PASP, 121, 1180

Mercer, E. P., Clemens, D. P., Meade, M. R., Babler, B. L., Indebetouw, R., Whitney, B. A., Watson, C., Wolfire, M. G., Wolff, M. J., Bania, T. M., Benjamin, R. A., Cohen, M., Dickey, J. M., Jackson, J. M., Kobulnicky, H. A., Mathis, J. S., Stauffer, J. R., Stolovy, S. R., Uzpen, B., & Churchwell, E. B. 2005, ApJ, 635, 560

Merrifield, M. R. 2004, in Milky Way Surveys: The Structure and Evolution of our Galaxy, Proc. of

ASP Conference 317, eds. D. Clemens, R. Shah, & T. Brainerd (San Francisco: ASP), 289

Mihalas, D., & Binney, J. 1981, Galactic Astronomy (San Francisco: W. H. Freeman & Co)

Minier, V., Ellingsen, S. P., Norris, R. P., & Booth, R. S. 2003, A&A, 403, 1095

Minniti, D., Lucas, P. W., Emerson, J. P., Saito, R. K., Hempel, M., Pietrukowicz, P., Ahumada, A. V., Alonso, M. V., Alonso-Garcia, J., Arias, J. I., Bandyopadhyay, R. M., Barbá, R. H., Barbuy, B., Bedin, L. R., Bica, E., Borissova, J., Bronfman, L., Carraro, G., Catelan, M., Clariá, J. J., Cross, N., de Grijs, R., Dékány, I., Drew, J. E., Fariña, C., Feinstein, C., Lajús, E. F., Gamen, R. C., Geisler, D., Gieren, W., Goldman, B., Gonzalez, O. A., Gunthardt, G., Gurovich, S., Hambly, N. C., Irwin, M. J., Ivanov, V. D., Jordán, A., Kerins, E., Kinemuchi, K., Kurtev, R., López-Corredoira, M., Maccarone, T., Masetti, N., Merlo, D., Messineo, M., Mirabel, I. F., Monaco, L., Morelli, L., Padilla, N., Palma, T., Parisi, M. C., Pignata, G., Rejkuba, M., Roman-Lopes, A., Sale, S. E., Schreiber, M. R., Schröder, A. C., Smith, M., Sodré, L., Soto, M., Tamura, M., Tappert, C., Thompson, M. A., Toledo, I., Zoccali, M., & Pietrzynski, G. 2010, New Astronomy, 15, 433

Misiriotis, A., Xilouris, E. M., Papamastorakis, J., Boumis, P., & Goudis, C. D. 2006, A&A, 459, 113

Mizuno, D. R., Kraemer, K. E., Flagey, N., Billot, N., Shenoy, S., Paladini, R., Ryan, E., Noriega-Crespo, A., & Carey, S. J. 2010, AJ, 139, 1542

Molinari, S., Swinyard, B., Bally, J., Barlow, M., Bernard, J.-P., Martin, P., Moore, T., Noriega-Crespo, A., Plume, R., Testi, L., Zavagno, A., Abergel, A., Ali, B., André, P., Baluteau, J.-P., Benedettini, M., Berné, O., Billot, N. P., Blommaert, J., Bontemps, S., Boulanger, F., Brand, J., Brunt, C., Burton, M., Campeggio, L., Carey, S., Caselli, P., Cesaroni, R., Cernicharo, J., Chakrabarti, S., Chrysostomou, A., Codella, C., Cohen, M., Compiegne, M., Davis, C. J., de Bernardis, P., de Gasperis, G., Francesco, J. D., di Giorgio, A. M., Elia, D., Faustini, F., Fischera, J. F., Fukui, Y., Fuller, G. A., Ganga, K., Garcia-Lario, P., Giard, M., Giardino, G., Glenn, J., Goldsmith, P., Griffin, M., Hoare, M., Huang, M., Jiang, B., Joblin, C., Joncas, G., Juvela, M., Kirk, J., Lagache, G., Li, J. Z., Lim, T. L., Lord, S. D., Lucas, P. W., Maiolo, B., Marengo, M., Marshall, D., Masi, S., Massi, F., Matsuura, M., Meny, C., Minier, V., Miville-Deschênes, M.-A., Montier, L., Motte, F., Müller, T. G., Natoli, P., Neves, J., Olmi, L., Paladini, R., Paradis, D., Pestalozzi, M., Pezzuto, S., Piacentini, F., Pomarès, M., Popescu, C. C., Reach, W. T., Richer, J., Ristorcelli, I., Roy, A., Royer, P., Russeil, D., Saraceno, P., Sauvage, M., Schilke, P., Schneider-Bontemps, N., Schuller, F., Schultz, B., Shepherd, D. S., Sibthorpe, B., Smith, H. A., Smith, M. D., Spinoglio, L., Stamatellos, D., Strafella, F., Stringfellow, G., Sturm, E., Taylor, R., Thompson, M. A., Tuffs, R. J., Umana, G., Valenziano, L., Vavrek, R., Viti, S., Waelkens, C., Ward-Thompson, D., White, G., Wyrowski, F., Yorke, H. W., & Zhang, Q. 2010, PASP, 122, 314

Momany, Y., Zaggia, S., Gilmore, G., Piotto, G., Carraro, G., Bedin, L. R., & de Angeli, F. 2006, A&A, 451, 515

Morgan, W. W., Whitford, A. E., & Code, A. D. 1953, ApJ, 118, 318

Murray, N., & Rahman, M. 2010, ApJ, 709, 424

Neugebauer, G., Habing, H. J., van Duinen, R., Aumann, H. H., Baud, B., Beichman, C. A., Beintema, D. A., Boggess, N., Clegg, P. E., de Jong, T., Emerson, J. P., Gautier, T. N., Gillett, F. C., Harris, S., Hauser, M. G., Houck, J. R., Jennings, R. E., Low, F. J., Marsden, P. L., Miley, G., Olnon, F. M., Pottasch, S. R., Raimond, E., Rowan-Robinson, M., Soifer, B. T., Walker, R. G., Wesselius, P. R., & Young, E. 1984, ApJ, 278, L1

Nishiyama, S., Nagata, T., Baba, D., Haba, Y., Kadowaki, R., Kato, D., Kurita, M., Nagashima, C., Nagayama, T., Murai, Y., Nakajima, Y., Tamura, M., Nakaya, H., Sugitani, K., Naoi, T., Matsunaga, N., Tanabé, T., Kusakabe, N., & Sato, S. 2005, ApJ, 621, L105

Nishiyama, S., Nagata, T., Sato, S., Kato, D., Nagayama, T., Kusakabe, N., Matsunaga, N., Naoi, T., Sugitani, K., & Tamura, M. 2006, ApJ, 647, 1093

Ohta, K., Hamabe, M., & Wakamatsu, K.-I. 1990, ApJ, 357, 71

Omont, A., Gilmore, G. F., Alard, C., Aracil, B., August, T., Baliyan, K., Beaulieu, S., Bégon, S., Bertou, X., Blommaert, J. A. D. L., Borsenberger, J., Burgdorf, M., Caillaud, B., Cesarsky, C., Chitre, A., Copet, E., de Batz, B., Egan, M. P., Egret, D., Epchtein, N., Felli, M., Fouqué, P., Ganesh, S., Genzel, R., Glass, I. S., Gredel, R., Groenewegen, M. A. T., Guglielmo, F., Habing, H. J., Hennebelle, P., Jiang, B., Joshi, U. C., Kimeswenger, S., Messineo, M., Miville-Deschênes, M. A., Moneti, A., Morris, M., Ojha, D. K., Ortiz, R., Ott, S., Parthasarathy, M., Pérault, M., Price, S. D., Robin, A. C., Schultheis, M., Schuller, F., Simon, G., Soive, A., Testi, L., Teyssier, D., Tiphène, D., Unavane, M., van Loon, J. T., & Wyse, R. 2003, A&A, 403, 975

Oort, J. H. 1977, ARAA, 15, 295

Paczynski, B. 1997, in Variables Stars and the Astrophysical Returns of the Microlensing Surveys,

eds. R. Ferlet, J.-P. Maillard, & B. Raban (Gif-sur-Yvette, France: Editions Frontieres), 357

Peretto, N. & Fuller, G. A. 2009, A&A, 505, 405

Phillips, J. P., & Ramos-Larios, G. 2008a, MNRAS, 386, 995

Phillips, J. P., & Ramos-Larios, G. 2008b, MNRAS, 383, 1029

Pidopryhora, Y., Lockman, F. J., & Shields, J. C. 2007, ApJ, 656, 928

Plambeck, R. L., & Menten, K. M. 1990, ApJ, 364, 555

Povich, M. S., Churchwell, E., Bieging, J. H., Kang, M., Whitney, B. A., Brogan, C. L., Kulesa, C. A., Cohen, M., Babler, B. L., Indebetouw, R., Meade, M. R., & Robitaille, T. P. 2009, ApJ, 696, 1278

Povich, M. S., Stone, J. M., Churchwell, E., Zweibel, E. G., Wolfire, M. G., Babler, B. L., Indebetouw, R., Meade, M. R., & Whitney, B. A. 2007, ApJ, 660, 346

Price, S. D., Egan, M. P., Carey, S. J., Mizuno, D. R., & Kuchar, T. A. 2001, AJ, 121, 2819

Purcell, C. R., Hoare, M. G., & Diamond, P. 2008, in Massive Star Formation: Observations Confront Theory: ASP Conference Series 387, eds. H. Beuther, H. Linz, & T. Henning (San Francisco: ASP), 389

Ragan, S. E., Bergin, E. A., & Gutermuth, R. A. 2009, ApJ, 698, 324

Reach, W. T., Rho, J., Tappe, A., Pannuti, T. G., Brogan, C. L., Churchwell, E. B., Meade, M. R., Babler, B., Indebetouw, R., & Whitney, B. A. 2006, AJ, 131, 1479

Reid, M. J. 1993, ARAA, 31, 345

Reid, M. J., Menten, K. M., Zheng, X. W., Brunthaler, A., & Xu, Y. 2009, ApJ, 705, 1548

Reipurth, B. 2008, Handbook of Star Forming Regions, Vol. 1: The Northern Sky (San Francisco: ASP Monograph Publications)

Reylé, C., Marshall, D. J., Robin, A. C., & Schultheisé, M. 2009, A&A, 495, 819

Rhoads, J. E. 1998, AJ, 115, 472

Rieke, G. H., Blaylock, M., Decin, L., Engelbracht, C., Ogle, P., Avrett, E., Carpenter, J., Cutri, R. M. et al. 1995, AJ, 135, 2245

Rix, H.-W., & Zaritsky, D. 1995, ApJ, 447, 82

Robin, A. C. 2009, A&A, 500, 165

Robin, A. C., Creze, M., & Mohan, V. 1992a, ApJ, 400, L25

Robin, A. C., Creze, M., & Mohan, V. 1992b, A&A, 265, 32

Robin, A. C., Reyle, C., Derriere, S. & Picaud, S. 2003, A&A, 409, 523

Robitaille, T. P., Cohen, M., Whitney, B. A., Meade, M., Babler, B., Indebetouw, R., & Churchwell, E. 2007a, AJ, 134, 2099

Robitaille, T. P., Whitney, B. A., Indebetouw, R., & Wood, K. 2007b, ApJSupp, 169, 328

Robitaille, T. P., Meade, M. R., Babler, B. L., Whitney, B. A., Johnston, K. G., Indebetouw, R., Cohen, M., Povich, M. S., Sewilo, M., Benjamin, R. A., & Churchwell, E. 2008, AJ, 136, 2413

Robitaille, T. P., & Whitney, B. A. 2010, ApJL, 710, L11

Robitaille, T. P., Churchwell, E., Benjamin, R. A., Whitney, B. A., Wood, K., Babler, B. L., & Meade, M. R. 2012, A&A, in press

Rodriguez-Fernandez, N. J., & Combes, F. 2008, A&A, 489, 115

Ruphy, S., Robin, A. C., Epchtein, N., Copet, E., Bertin, E., Fouque, P., & Guglielmo, F. 1996, A&A, 313, L21

Sackett, P. D. 1997, ApJ, 483, 103

Salpeter, E. E. 1955, ApJ, 121, 161

Sawada, T., Hasegawa, T., Handa, T., & Cohen, R. J. 2004, MNRAS, 349, 1167

Schweizer, F. 1976, ApJ Supp, 31, 313

Scoville, N. Z., & Solomon, P. M. 1975, ApJ, 199, L105

Seigar, M. S., & James, P. A. 1998, MNRAS, 299, 685

Sevenster, M. N. 1999, MNRAS, 310, 629

Shu, F. H., Milione, V., & Roberts, W. W. 1973, ApJ, 183, 819

Simon, R., Jackson, J. M., Rathborne, J. M., & Chambers, E. T. 2006, ApJ, 639, 227

Skrutskie, M. F., Cutri, R. M., Stiening, R., Weinberg, M. D., Schneider, S., Carpenter, J. M., Beichman, C., Capps, R., Chester, T., Elias, J., Huchra, J., Liebert, J., Lonsdale, C., Monet, D. G., Price, S., Seitzer, P., Jarrett, T., Kirkpatrick, J. D., Gizis, J. E., Howard, E., Evans, T., Fowler, J., Fullmer, L., Hurt, R., Light, R., Kopan, E. L., Marsh, K. A., McCallon, H. L., Tam, R., Dyk, S. V., & Wheelock, S. 2006, AJ, 131, 1163

Smith, L. F., Biermann, P., & Mezger, P. G. 1978, A&A, 66, 65

Srinivasan, S., Meixner, M., Leitherer, C., Vijh, U., Volk, K., Blum, R. D., Babler, B. L., Block, M., Bracker, S., Cohen, M., Engelbracht, C. W., For, B.-Q., Gordon, K. D., Harris, J., Hora, J. L., Indebetouw, R., Markwick-Kemper, F., Meade, M., Misselt, K. A., Sewilo, M., & Whitney, B. 2009, AJ, 137, 4810

Stead, J. J., & Hoare, M. G. 2010, MNRAS, 407, 923

Su, K. Y. L., Chu, Y.-H., Rieke, G. H., Huggins, P. J., Gruendl, R., Napiwotzki, R., Rauch, T., Latter, W. B., & Volk, K. 2007, ApJ, 657, L41

Su, K. Y. L., Kelly, D. M., Latter, W. B., Misselt, K. A., Frank, A., Volk, K., Engelbracht, C. W., Gordon, K. D., Hines, D. C., Morrison, J. E., Muzerolle, J., Rieke, G. H., Stansberry, J. A., & Young, E. 2004, ApJSupp, 154, 302

Tielens, A. G. G. M. 2005, The Physics and Chemistry of the Interstellar Medium, (Cambridge, UK: Cambridge University Press)

Ueta, T. 2006, ApJ, 650, 228

van der Kruit, P. C., & Searle, L. 1981, A&A, 95, 105

van Loon, J. T., Gilmore, G. F., Omont, A., Blommaert, J. A. D. L., Glass, I. S., Messineo, M., Schuller, F., Schultheis, M., Yamamura, I., & Zhao, H. S. 2003, MNRAS, 338, 857

van Woerden, H., Rougoor, G. W., & Oort, J. H. 1957, Comptes Rendus l'Academie des Sciences, 244, 1691

Vanhollebeke, E., Groenewegen, M. A. T., & Girardi, L. 2009, A&A, 498, 95

Vig, S., Ghosh, S. K., & Ojha, D. K. 2005, A&A, 436, 867

Wachter, S., Mauerhan, J. C., van Dyk, S. D., Hoard, D. W., Kafka, S., & Morris, P. W. 2010, AJ, 139, 2330

Wainscoat, R. J., Cohen, M., Volk, K., Walker, H. J., & Schwartz, D. E. 1992, ApJSupp, 83, 111

Ward-Thompson, D. 1994, in Clouds; cores and low mass stars: ASP Conference Series 65, eds. D. Clemens & R. Barvainis (San Francisco: ASP), 207

Watson, C., Povich, M. S., Churchwell, E. B., Babler, B. L., Chunev, G., Hoare, M., Indebetouw, R., Meade, M. R., Robitaille, T. P., & Whitney, B. A. 2008, ApJ, 681, 1341

Weinberg, M. D. 1992, ApJ, 384, 81

Weingartner, J. C., & Draine, B. T. 2001, ApJ, 548, 296

Westerhout, G. 1957, Bulletin of the Astronomical Institutes of the Netherlands, 13, 201

Whitney, B. 2009, BAAS, 41, 715

Whitney, B. A., Indebetouw, R., Bjorkman, J. E., & Wood, K. 2004, ApJ, 617, 1177

Whittet, D. C. B. 2003, Dust in the galactic environment (Bristol: IOP Publishing)

Williams, J. P., de Geus, E. J., & Blitz, L. 1994, ApJ, 428, 693

Wozniak, P. R., Udalski, A., Szymanski, M., Kubiak, M., Pietrzynski, G., Soszynski, I., & Zebrun, K. 2002, Acta Astronomica, 52, 129

Wright, E. L., Eisenhardt, P. R. M., Mainer, A., Ressler, M. E., Cutri, R. M., Jarrett, T., Kirkpatrick, J. D., et al. 2010, AJ, 140, 1868

Yanny, B., Rockosi, C., Newberg, H. J., Knapp, G. R., Adelman-McCarthy, J. K., Alcorn, B., Allam, S., Prieto, C. A., An, D., Anderson, K. S. J., Anderson, S., Bailer-Jones, C. A. L., Bastian, S., Beers, T. C., Bell, E., Belokurov, V., Bizyaev, D., Blythe, N., Bochanski, J. J., Boroski, W. N., Brinchmann, J., Brinkmann, J., Brewington, H., Carey, L., Cudworth, K. M., Evans, M., Evans, N. W., Gates, E., Gänsicke, B. T., Gillespie, B., Gilmore, G., Gomez-Moran, A. N., Grebel, E. K., Greenwell, J., Gunn, J. E., Jordan, C., Jordan, W., Harding, P., Harris, H., Hendry, J. S., Holder, D., Ivans, I. I., Ivezič, Ž., Jester, S., Johnson, J. A., Kent, S. M., Kleinman, S., Kniazev, A., Krzesinski, J., Kron, R., Kuropatkin, N., Lebedeva, S., Lee, Y. S., Leger, R. F., Lépine, S., Levine, S., Lin, H., Long, D. C., Loomis, C., Lupton, R., Malanushenko, O., Malanushenko, V., Margon, B., Martinez-Delgado, D., McGehee, P., Monet, D., Morrison, H. L., Munn, J. A., Neilsen, E. H., Nitta, A., Norris, J. E., Oravetz, D., Owen, R., Padmanabhan, N., Pan, K., Peterson, R. S., Pier, J. R., Platson, J., Fiorentin, P. R., Richards, G. T., Rix, H.-W., Schlegel, D. J., Schneider, D. P., Schreiber, M. R., Schwope, A., Sibley, V., Simmons, A., Snedden, S. A., Smith, J. A., Stark, L., Stauffer, F., Steinmetz, M., Stoughton, C., Rao, M. S., Szalay, A., Szkody, P., Thakar, A. R., Thirupathi, S., Tucker, D., Uomoto, A., Berk, D. V., Vidrih, S., Wadadekar, Y., Watters, S., Wilhelm, R., Wyse, R. F. G., Yarger, J., & Zucker, D. 2009, AJ, 137, 4377

Zasowski, G., Majewski, S. R., Indebetouw, R., Meade, M. R., Nidever, D. L., Patterson, R. J., Babler, B., Skrutskie, M. F., Watson, C., Whitney, B. A., & Churchwell, E. 2009, ApJ, 707, 510

Zoccali, M. 2010, in Chemical Abundances in the Universe: Connecting First Stars to Planets, IAU Symposium 265, 271

Zwicky, F. 1955, PASP, 67, 232